



CD44-targeted nanoparticles for co-delivery of docetaxel and an Akt inhibitor against colorectal cancer

Juan Gonzalez-Valdivieso^a, Reinaldo Vallejo^{a,b}, Soraya Rodriguez-Rojo^b, Mercedes Santos^c, Jose Schneider^{a,d}, Francisco Javier Arias^{a,e,*}, Alessandra Girotti^{a,e,*}

^a Smart Devices for NanoMedicine Group, University of Valladolid, LUCIA Building, Valladolid, Spain

^b BioEcoUVa, Research Institute on Bioeconomy, High Pressure Process Group, University of Valladolid, Department of Chemical Engineering and Environmental Technology, Escuela de Ingenierías Industriales, Sede Mergelina, Valladolid, Spain

^c BIOFORGE Research Group (Group for Advanced Materials and Nanobiotechnology), University of Valladolid, CIBER-BBN, LUCIA Building, Valladolid, Spain

^d Department of Obstetrics & Gynecology, University of Valladolid, School of Medicine, Valladolid, Spain

^e Unidad de excelencia Instituto de Biomedicina y Genética Molecular de Valladolid (IBGM), University of Valladolid CSIC, Valladolid, Spain

ARTICLE INFO

Keywords:

Nanomedicine
Drug delivery
Nanoparticles
Biomaterials
Elastin-like recombinamers (ELRs)
Colorectal cancer (CRC)

ABSTRACT

New strategies to develop drug-loaded nanocarriers with improved therapeutic efficacy are needed for cancer treatment. Herein we report a novel drug-delivery nanosystem comprising encapsulation of the chemotherapeutic drug docetaxel (DTX) and recombinant fusion of a small peptide inhibitor of Akt kinase within an elastin-like recombinamer (ELR) vehicle. This combined approach is also precisely targeted to colorectal cancer cells by means of a chemically conjugated DNA aptamer specific for the CD44 tumor marker. This 53 nm dual-approach nanosystem was found to selectively affect cell viability (2.5 % survival) and proliferation of colorectal cancer cells *in vitro* compared to endothelial cells (50 % survival), and to trigger both apoptosis- and necrosis-mediated cell death. Our findings also show that the nanohybrid particles remain stable under physiological conditions, trigger sustained drug release and possess an adequate pharmacokinetic profile after systemic intravenous administration. *In vivo* assays showed that these dual-approach nanohybrids significantly reduced the number of tumor polyps along the colorectal tract in a murine colorectal cancer model. Furthermore, systemic administration of advanced nanohybrids induced tissue recovery by improving the morphology of gastrointestinal crypts and the tissue architecture. Taken together, these findings indicate that our strategy of an advanced dual-approach nanosystem allows us to achieve successful controlled release of chemotherapeutics in cancer cells and may have a promising potential for colorectal cancer treatment.

1. Introduction

Colorectal cancer (CRC) is one of the most commonly diagnosed cancers worldwide [1,2]. Several factors can explain both the high incidence and mortality of colorectal cancer, including genetic predisposition, environmental aspects, coexistence of other diseases, or late detection of this cancer [3]. Current strategies against CRC are based on two different approaches, namely early diagnosis and prevention of the disease in populations with increased risk factors or other related diseases [4], and the use of surgery and chemotherapeutic agents. However, the most commonly used drugs nowadays, such as oxaliplatin and 5-FU, pose several problems in terms of lack of selectivity and undesired side effects [5]. As such, novel approaches exploring new drugs and

promising targets are needed [6–8].

Among these novel strategies, biomaterials are able to overcome the limitations of current drugs and are therefore one of the most encouraging therapeutic approaches [9,10]. Elastin-like recombinamers (ELRs) are protein-based polymers based on repetition of the VPGXG pentapeptide found in the sequence of natural elastin, where X can be substituted by any amino acid except proline [11]. Moreover, recombinant DNA technology allows us to achieve full control over the ELR sequence and include bioactive sequences [12]. ELRs also present excellent biocompatibility and biodegradability, and show stimulus-responsive behavior [13]. These characteristics, together with their lack of immunogenicity, mean that ELRs have attracted exceptional interest among the multiple different types of biomaterials [14,15], with

* Corresponding authors at: Smart Devices for Nanomedicine Group, University of Valladolid, Lucia Building, Valladolid, Spain.

E-mail addresses: arias@bio.uva.es (F.J. Arias), alessandra.girotti@uva.es (A. Girotti).

<https://doi.org/10.1016/j.bioadv.2023.213595>

Received 20 February 2023; Received in revised form 24 July 2023; Accepted 19 August 2023

Available online 21 August 2023

2772-9508/© 2023 Published by Elsevier B.V.

potential applications in gene and drug delivery, tissue engineering, 3D bioprinting, cell harvesting, etc. [16–18].

Herein we report the development of advanced nanohybrids as dual-approach drug-delivery systems containing two different therapeutic agents to counteract the partial inefficiency of each treatment due to tumor heterogeneity. Thus, these nanohybrids include a small peptide inhibitor (Akt-in) of Akt phosphorylation. Akt is an intracellular kinase involved in cell proliferation, growth and survival, and is overexpressed in multiple types of cancer, such as colon, pancreatic, lung, breast and ovarian cancer, among others [19,20]. In particular, this inhibitor has been shown to prevent the anti-apoptotic action of Akt protein involved in cancer cell proliferation and tumor progression [21–23]. Genetic engineering techniques allowed us to include the inhibitor as well as specific bioactive sequences in ELR-based nanoparticles, thereby modulating the intracellular delivery of Akt-in [22]. Secondly, the chemotherapeutic agent docetaxel (DTX) was encapsulated within ELR-based nanohybrids. DTX is a well-known antimetabolic agent that is used clinically to treat breast, ovarian, colorectal, lung, and head and neck cancer [24,25]. As DTX is highly hydrophobic and shows non-specific efficacy, encapsulation is an encouraging approach to allow selective delivery and increase drug concentration within cancer cells to achieve more successful response rates in tumor treatments [26–28].

This work was intended to develop an advanced dual-approach therapeutic system for application in colorectal cancer. Recombinant DNA technology and SAS allowed us to develop smart nanohybrids carrying the Akt inhibitor and DTX to specifically release both these anti-tumor drugs inside the target cancer cells. Although targeted nanoparticles have previously been used against colorectal cancer, this is the first time that a drug delivery system combining a clinically used drug (DTX) and a promising therapeutic peptide (Akt inhibitor) is evaluated *in vitro* and *in vivo* as a novel strategy for CRC therapy.

2. Materials and methods

2.1. Materials, chemical reagents and cell lines

E. coli BLR (DE3) strain was purchased from Merck. Minimum essential medium (MEM), fetal bovine serum (FBS), penicillin streptomycin solution, trypsin-EDTA, DPBS, glutamine, non-essential amino acids (NEAA), LIVE/DEAD® Viability/Cytotoxicity Kit for mammalian cells, Annexin V FITC Assay Kit, Eosin and Gill 3 Haematoxylin were supplied by Invitrogen. Carbon dioxide (99.95 % purity) was supplied by Carbueros Metálicos S.A. Docetaxel was provided by Apollo Scientific with a purity of 99 %. Dimethyl sulfoxide (DMSO; ≥99.7 % purity), deuterium oxide (99.9 atom % D purity), human colorectal cancer cells (Caco-2, 86,010,202 ECACC), paraformaldehyde, Triton X-100, rhodamine, azoxymethane (AOM) and Eukitt mounting medium were purchased from Sigma–Aldrich. Dextran sodium sulfate (molecular weight 36.000–50.000 Da.) was purchased from MP Biomedicals. Human umbilical vein endothelial cells (HUVEC, cc-2517), medium 200, low serum growth supplement (LSGS) and gentamicin/amphotericin solution were acquired from Gibco. Isoflurane was purchased from Esteve, and ethanol and xylene from Scharlau.

The azide-modified DNA aptamer for specific binding to CD44 (5'-C3-azide-GAGATTCATCACGCGCA-TAGTCCCAAGGCCTGCAAGGGAACCAAGGACACAGCGACTATGCGA-3') was purchased from Metabion.

2.2. ELR bioproduction and purification

The ELRs used in this work were bioproduced as described previously [29]. The final genes were constructed by sequential introduction of monomer gene segments in a stepwise manner using the recursive directional ligation method. The DNA sequence was verified by DNA sequencing. After transformation of expression vectors containing the selected ELR genes into *E. coli* BLR (DE3) strain, ELRs were bioproduced

in *E. coli* in a 15 L bioreactor (Applikon Biotechnology, the Netherlands) and purified by cooling/heating cycles (inverse transition cycling) taking advantage of their thermoresponsive behavior. Polymers were obtained in a yield of approximately 50 mg per litre of bacterial culture. Endotoxins were removed by performing additional NaCl and NaOH treatments [30]. The final ELR was then dialyzed against ultrapure water type I, sterilized by filtration (0.22 µm filters, Nalgene) and freeze-dried prior to storage. Sodium dodecyl sulfate polyacrylamide gel electrophoresis (SDS-PAGE) and matrix-assisted laser desorption ionization time-of-flight mass spectrometry (MALDI-TOF/MS) were performed to determine the molecular weight and purity, respectively. Moreover, the amino acid composition was determined by high-performance liquid chromatography (HPLC) and nuclear magnetic resonance (NMR) spectroscopy by the Laboratory of Instrumental Techniques at the University of Valladolid (Spain).

2.3. Chemical modification and DNA aptamer functionalization by click chemistry

ELR polymers were functionalized with NHS-PEG-cyclooctyne by way of an amidation reaction between the ε-amine group from lysines present in the polymers and the activated carboxylic group as the *N*-succinimidyl ester of NHS-PEG-cyclooctyne.

Briefly, one equivalent of ELR was mixed with 0.33 equivalents of NHS-PEG-cyclooctyne ((2,5-dioxopyrrolidin-1-yl-1-((1*R*,8*S*,9*S*)-bicyclo(6.1.0)non-4-yn-9-yl)-3,14-dioxo-2,7,10-trioxo-4-13-diazaoctadecan-18-oate) (3 mg/mL) in DMF under a nitrogen atmosphere at room temperature. The mixture was stirred overnight at 4 °C, dialyzed against cold ultrapure water type I and lyophilized. The incorporation of PEG as ELR-PEG-cyclooctyne to the ELR was evaluated by ¹H NMR spectroscopy.

For aptamer functionalization by click chemistry, one equivalent of CD44-Azide was mixed with one equivalent of ELR-PEG-cyclooctyne previously dissolved in ultrapure water type I (pH 7.4) and the mixture was left at 4 °C for 24 h. The product was then dialyzed against cold ultrapure water type I and lyophilized. The incorporation of CD44 aptamer by cycloaddition of azide and activated cyclooctyne was corroborated by spectrophotometry, measuring the absorbance at 260 nm with a Nanodrop 2000 instrument (Thermo Scientific, USA).

2.4. Supercritical antisolvent process

The supercritical antisolvent (SAS) technique uses supercritical CO₂ to encapsulate DTX in the previously described ELR polymers to produce nanohybrid particles. For this purpose, the methodology and operating conditions reported previously by our laboratory were used [31]. Briefly, the ELRs and DTX were dissolved in DMSO and, once the operating conditions had been reached, the solution was pumped into the reactor through a coaxial nozzle. After drying the particles with fresh CO₂, they were collected and stored at 4 °C for further characterization and analysis.

2.5. Calculation of component proportions

The spectra were analyzed to calculate the ELR:DMSO and DTX ratio within the nanohybrids. Thus, samples were dissolved in D₂O at 2 mg/mL and a total of 256 scans per sample were performed. NMR data were acquired using an Agilent 400 NMR spectrometer (Laboratory of Instrumental Techniques, University of Valladolid, Spain). The proportions of the different components were obtained by comparing the integral of the signal for the methyl groups from the ELR with those for the protons in the aryl moieties of DTX and the methyl groups of DMSO. Spectra were analyzed using MestReNova v9.0.1 software (Mestrelab Research, USA).

2.6. Size and ζ -potential

The size and ζ -potential of the ELR-based nanohybrids were measured by dynamic light scattering (DLS) using a Zetasizer Nano ZS (Malvern Instruments Ltd., UK) at 37 °C. Solutions were prepared by dissolving the ELRs in PBS (pH 7.4) or 1 mM NaCl ultrapure water type I (pH 7.4), when indicated, and then filtered using a 0.45 μ m poly(vinylidene difluoride) (PVDF) syringe filter. Samples were incubated for 30 min at 37 °C to allow supramolecular assembly and then introduced into polystyrene cuvettes and stabilized for 2 min at 37 °C. Autocorrelation functions were used to obtain the size distribution and polydispersity index (PDI). Z-average mean (nm) and ζ -potential (mV) were used for data analysis. Three different samples of each type of nanohybrid were analyzed.

For interaction assays, ELR nanohybrids were incubated in 5 % BSA-containing PBS at 37 °C for 24 h and then filtered, introduced into polystyrene cuvettes and stabilized for 2 min at 37 °C. Autocorrelation functions were used to obtain the size distribution and polydispersity index. Z-average mean (nm) values were used for data analysis. Three different samples of each type of nanohybrid were analyzed.

2.7. Transmission electron microscopy (TEM)

Solutions were prepared by dissolving the ELRs in ultrapure water type I (pH 7.4) followed by incubation for 30 min at 37 °C to allow supramolecular assembly. The samples were then stained with uranyl acetate solution (1.0 wt%) to enhance the contrast of the nanohybrids on a carbon-coated copper grid, and the solvent was evaporated. Samples were observed using a JEM-2200 electron microscope (JEOL, Japan) operating at 200 kV at UVa Scientific Park, University of Valladolid, Spain.

2.8. Atomic Force Microscopy (AFM)

Samples were prepared by placing 50 μ L of the ELR at a concentration of 1 mg/mL, stabilized at 37 °C in PBS, on mica, followed by water evaporation at the same temperature. AFM was performed in air at 25 °C using a MFP-3D Bio Asylum Research system (Oxford Instruments, UK) attached to a Nikon Ti2 microscope in tapping mode at the Laboratory of Instrumental Techniques (University of Valladolid, Spain). Asylum Research AR 16.12.214 software (Oxford Instruments, UK) was used for data treatment.

2.9. *In vitro* release studies

The experimental procedure to acquire the drug-delivery profiles was carried out as described previously [31]. Briefly, *in vitro* drug-delivery experiments were performed in triplicate at 37 °C using the dialysis method by dispersing 1 mg of targeted nanoparticles (tNPs+DTX and tNPs Ai+DTX) in 1 mL of PBS release medium. The control sample was prepared from free DTX at the highest concentration reached of 0.06 mg/mL in the same release medium. Previously activated dialysis bags (MWCO 12 kD) were filled with 1 mL of each solution and sealed at both ends. These bags were then immersed in 30 mL glass vials, previously filled with 20 mL of release medium. The content of these vials was stirred at 80 rpm and 37 °C in an incubator throughout the experiment. A 1 mL sample was withdrawn from the release medium at predetermined time intervals and the same volume of fresh medium added to maintain sink conditions.

The amount of DTX released with time was determined by UV/Vis spectrometry (UV/Vis spectrometer lambda 25, Perkin Elmer, UK) according to the Lambert–Beer law, at a wavelength of 234 nm. A calibration curve was plotted beforehand using solutions of DTX dissolved in PBS at a concentration of between 50 and 3.125 μ g/mL.

To analyze the mechanism of drug release-rate kinetics, the results of *in vitro* release profiles were fitted with the Lindner–Lippold and

Peppas–Sahlin mathematical models described previously [31].

2.10. Cell culture

Caco-2 colorectal cancer cells were grown in MEM supplemented with 10 % FBS, 2 mM glutamine, 1 % NEAA, 100 U/mL penicillin and 0.1 mg/mL streptomycin at 37 °C and 5 % CO₂. Human umbilical vein endothelial cells (HUVEC) were maintained in Medium 200 supplemented with 1 % gentamicin/amphotericin and low serum growth supplement (LSGS) at 5 % CO₂ and 37 °C. Cells were harvested using a solution of 0.05 % Trypsin-EDTA, when required. Cells were seeded onto 96-well plates (2 \times 10⁴ cells per cm² and 1 \times 10⁴ cells per cm² for tumor and primary endothelial cells, respectively) and incubated for 24 h before treatment in order to maintain similar levels of confluence.

2.11. Cell proliferation

To determine the effectiveness of the DNA aptamer conjugation, Caco-2 and HUVEC were treated with ELRs at three different concentrations (0.25, 0.5 and 1 mg/mL) and incubated for 72 h.

For the assays involving ELR nanohybrids, Caco-2 and HUVEC were treated with 1 μ M free DTX or ELR nanohybrids at equivalent normalized concentrations and incubated for 72 h.

Confluence percentages were determined every 4 h using the Cytosmart OMNI live-cell imaging microscope (Cytosmart, the Netherlands). Additional confluence percentages were determined every hour during the first 6 h. Three independent experiments were performed, each in triplicate.

2.12. Cell viability

Caco-2 and HUVEC were incubated with 1 μ M free DTX or ELRs at equivalent normalized concentrations for 30 min and 24 h. Live and dead staining (LIVE/DEAD Viability/Cytotoxicity Assay Kit) was used following the manufacturer's instructions. Briefly, a stock solution of 1 μ M calcein AM and 2 μ M EthD-1 in 10 mL of DPBS was prepared, then a 100 μ L aliquot was added to each well and incubated for 20 min in the dark. The fluorescence intensity emission was measured at 525 and 645 nm after excitation at 485 and 525 nm using a SpectraMax M5e microplate reader (Molecular Devices, USA). Three independent experiments were performed, each in triplicate.

2.13. Apoptosis/necrosis assay

Caco-2 and HUVEC cells were incubated with 1 μ M free DTX or ELR nanohybrids at equivalent normalized concentrations for 30 min or 24 h. Cells were stained with FITC-conjugated annexin V and propidium iodide (Annexin V FITC Assay Kit, Cayman Chemical) following the manufacturer's instructions and the fluorescence intensity emission was measured using a SpectraMax M5e microplate reader (Molecular Devices, USA) at 535 and 595 nm after excitation at 488 and 560 nm, respectively. Three independent experiments were performed, each in triplicate.

2.14. Confocal microscopy

Caco-2 cells were seeded on Millicell™ EZ Slides. After 24 h, these cells were incubated with rhodamine-loaded ELR nanohybrids for 1 h, then washed with PBS 1X, fixed with PFA 4 % and permeabilized with Triton 0.1 %. DAPI staining was used for cellular nuclei. Images were taken with a Leica TCS SP8 X confocal microscope (Leica microsystems, Germany) at the Laboratory of Instrumental Techniques (University of Valladolid, Spain).

2.15. *In vivo* pharmacokinetic analysis

All animal experiments were conducted according to the institutional guidelines for the care and use of experimental animals of the University of Valladolid (Spain) in accordance with Directive 2010/63/EU (Resolution Number 2010/2/23) under the supervision of the Animal Research and Welfare Committee.

BALB/c mice aged 14–16 weeks ($n = 5$) were intravenously injected via the tail vein with 100 μL of rhodamine-loaded ELR nanohybrids (tNPs-Ai-DTX-Rho) previously dissolved at 3 mg/mL. For the time course analysis, 20 μL of blood was collected at 1, 2, 3, 4, 5, 6 and 24 h post-injection and immediately diluted in 80 μL of heparinized PBS. The blood was centrifuged at 21,100 $\times g$ for 10 min at 4 $^{\circ}\text{C}$ and the supernatant was loaded onto a black clear-bottomed 96-well plate. The fluorescence intensity was read using a SpectraMax M5e microplate reader (Molecular Devices, USA) with excitation and emission wavelengths of 553 and 627 nm, respectively. Plasma auto fluorescence was determined from negative control (non-injected) mice and subtracted from the sample values. The fluorescence intensity values were converted to concentration by extrapolation using a linear standard curve.

To obtain the pharmacokinetic parameters, each individual mouse was fitted to a one-compartment pharmacokinetic model using SAAM II software (University of Washington, USA).

2.16. *In vivo* tumor induction

Tumor induction was performed as described previously by Neufert et al. [32]. Briefly, BALB/c mice ($n = 72$) aged 6–8 weeks were injected intraperitoneally with 7.5 mg/kg azoxymethane (AOM). Five days later, these mice were treated with 3 % dextran sodium sulfate (DSS) in drinking water for 5 days, followed by 15 days of regular drinking water. DSS treatment was repeated twice (three cycles of DSS were provided in total). The experimental time-course for tumor induction is depicted in Fig. 8A. Body weight and animal welfare were measured during the experiment.

2.17. *In vivo* magnetic resonance imaging (MRI)

MRI was performed at the Laboratory of Instrumental Techniques (University of Valladolid, Spain) using a 9.4 T 160 mm Bore Actively Screened MRI system (Agilent Technologies, USA) equipped with 400 mT/m gradient inserts and a 15 mm volume resonator RF coil (RAPID Biomedical, Germany). For the preliminary tumor induction assay, MRI was performed after animal sacrifice. For the assessment of anti-tumor efficacy of ELR nanohybrids, MRI was performed at day 25 post-treatment. Animals were anaesthetized with isoflurane in oxygen (4 % for induction and 1.5 % for maintenance).

2.18. *In vivo* anti-tumor efficacy

After the last DSS cycle for tumor induction, BALB/c mice were randomly divided (Table S4) into twelve groups (6 mice in each) and the treatment started, which is considered as day 0. The experimental groups were as follows: placebo group (mice treated with PBS), control empty ELR nanohybrids (tNPs [2 mg/kg]), free DTX 5 mg/kg, free DTX 2 mg/kg, nanohybrids only containing DTX 2 mg/kg (tNPs-DTX 2 mg/kg), nanohybrids only containing Akt inhibitor (tNPs-Ai [2 mg/kg]) and three groups for dual-approach treatments: high-dose group (tNPs-Ai-DTX 5 mg/kg), medium-dose group (tNPs-Ai-DTX 2 mg/kg) and low-dose group (tNPs-Ai-DTX 1 mg/kg). Furthermore, three multidose groups were also established: low dose in two injections (tNPs-Ai-DTX 1 mg/kg /2), medium dose in four injections (tNPs-Ai-DTX 2 mg/kg /4) and medium dose in six injections (2 mg/kg /6). The use of square brackets in tNP [2 mg/kg] and tNP-Ai [2 mg/kg] group names means that these groups were administered the equivalent amount of ELR as the tNPs-DTX 2 mg/kg group. Animals were injected intravenously with

PBS, free DTX or ELR nanohybrids at indicated concentrations via the tail vein, with the dose being adjusted to the group average weight. One month later, which corresponded to 95 days from the beginning of the tumor induction protocol, the mice were euthanized, and their colons extracted after necropsy. Tumor polyps were also counted and measured. Representative images of tumor polyps were taken using a Leica DMS 1000 microscope.

2.19. Tissue processing and histological staining

Colons were fixed with PFA 4 % and subsequently dehydrated by immersion in graded ethanol solutions from 70 % to 100 %, finishing with two passages in xylene solution. Samples were embedded in paraffin and then serially sliced into 5 μm sections using a microtome. Histological sections were transferred onto glass microscopy slides, then deparaffinized and rehydrated with subsequent immersion in xylene, graded ethanol solutions of decreasing concentration and distilled water. Samples were stained with haematoxylin-eosin (H&E).

2.20. Statistical analysis

Data are reported as mean \pm SD ($n = 3$). Statistical analysis involved a variance analysis in combination with a subsequent analysis using the Bonferroni method. A p value of <0.05 was considered to be statistically significant. $*p < 0.05$, $**p < 0.01$, $***p < 0.001$. Data were handled using the SPSS Statistics software version 20 (IBM, USA).

3. Results and discussion

3.1. ELR nanohybrids design

In previous studies we developed two different therapeutic nanoparticles designed to specifically tackle cancer cells by unlocking the apoptotic pathway blocked by Akt kinase [21,22] and releasing the antimetabolic drug DTX in cancer cells [31], respectively. Indeed, we demonstrated that both types of ELR nanoparticles reduced the cytotoxic effect on non-cancer cells, one of the most important challenges when developing novel therapeutic agents.

However, cancer is a complex disease with high variability between cell populations inside the same tumor. For this reason, the most promising therapies are based on a combination of multiple strategies in order to attack cancer cells in different ways, such as surgery, radiotherapy, chemotherapy or immunotherapy. Since drug encapsulation is an encouraging strategy that can be used to develop new therapeutic treatments, we designed novel hybrid ELR nanodevices to develop a dual-approach drug delivery system (Fig. 1). Thus, this strategy would combine two different therapeutic agents in the same vehicle to tackle tumor growth in two ways, namely inhibition of Akt phosphorylation (pro-apoptotic effect) and DTX encapsulation (anti-mitotic effect). For this purpose, we used the previously described recombinamers consisting of an amphiphilic ELR backbone including several bioactive sequences to deliver a small peptide Akt inhibitor [22]. This ELR polymer was able to self-assemble into highly monodisperse nanoparticles that can enter cancer cells as a result of clathrin-mediated endocytosis and release the Akt inhibitor in the cell cytoplasm, thus allowing the inhibitor to block Akt phosphorylation and subsequent activation, thereby triggering apoptosis-mediated cell death [21,22].

Secondly, we used an amphiphilic tetrablock [31] that is able to encapsulate DTX and diminish breast cancer cell viability. The block composition of the ELR polymers designed, and the resulting hybrid nanoparticles, is depicted in Fig. 1 and Table S1. The cytotoxic agents were chosen because Akt is one of the most dysregulated cell pathways within cancer cells while DTX is a gold standard chemotherapeutic drug in oncology. The DTX concentration (1 μM) was selected based on previous works [28,33].

Furthermore, ELR hybrid polymers were specifically targeted to

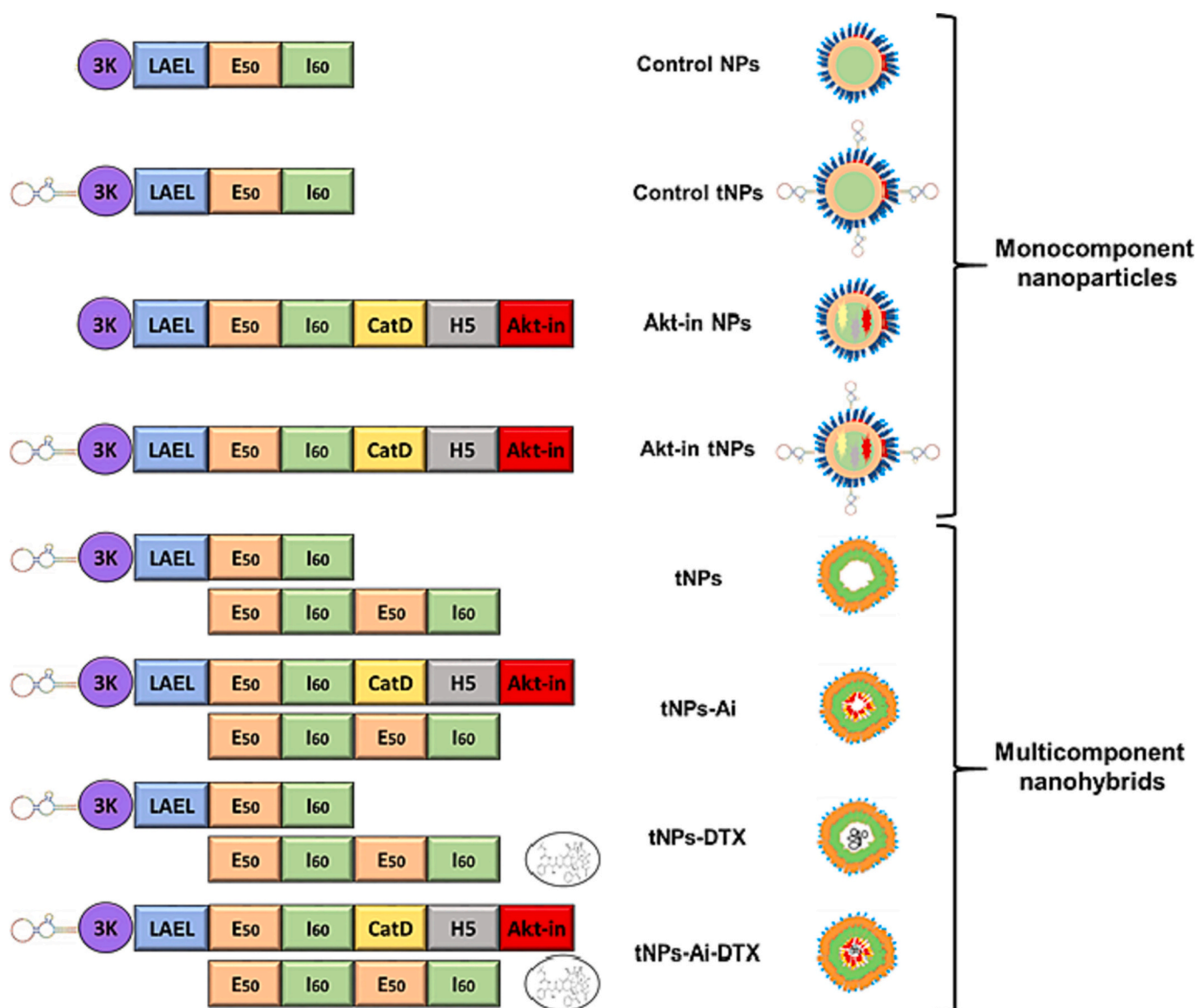


Fig. 1. Composition of hybrid ELR-based targeted nanoparticles (tNPs) including the anti-CD44 DNA aptamer. From top to bottom: Control NPs: nanoparticles lacking therapeutic molecules as negative control; Control tNPs: targeted nanoparticles lacking therapeutic molecules; Akt-in NPs: nanoparticles containing the Akt inhibitor; Akt-in tNPs: targeted nanoparticles containing the Akt inhibitor; tNPs: targeted nanohybrids lacking therapeutic molecules as negative control; tNPs-Ai: targeted nanohybrids containing the Akt inhibitor; tNPs-DTX: DTX encapsulated within targeted nanohybrids; tNPs-Ai-DTX: targeted nanohybrids containing both therapeutic agents (Akt inhibitor and DTX). Non-scaled scheme.

CD44, which is a membrane receptor located on the cell surface [34,35], and an established cancer marker due to its high expression in multiple tumors, such as colon, pancreatic, breast and head and neck cancer [36,37]. Thus, CD44 could be a good strategy for specifically releasing both Akt inhibitor and DTX inside cancer cells, thereby avoiding cytotoxic effects on normal tissues exposed during nanohybrid administration.

3.2. DNA aptamer conjugation

Although many different moieties can be used as targeting systems for the specific entry of nanoparticles into cancer cells, we selected a DNA aptamer [38,39] specifically designed to interact with CD44 [40] to release both Akt inhibitor and DTX inside cancer cells due to its higher affinity than the hyaluronic acid.

By taking advantage of click chemistry [41], the DNA aptamer was covalently linked to the lysine residues within the ELR sequence previously modified with PEG, which acted as a spacer between the aptamer

and the polymer, thereby facilitating the interaction between the DNA aptamer and CD44 receptor (Fig. S1).

The correct binding of NHS-PEG-cyclooctyne was confirmed by ^1H NMR spectroscopy (Fig. S1A), as new signals from PEG-cyclooctyne appeared at 3.0 ppm (methylene groups adjacent to the nitrogen of lysine thereby forming the new amide bond), 4.0 ppm (methylene group adjacent to carbamate and cyclopropyl group) and 7.0 ppm (H—N from carbamate). These three signals allowed us to verify the presence of NHS-PEG-cyclooctyne along the peptide chain. The presence of the DNA aptamer was confirmed by measuring the absorbance at 260 nm. As shown in Fig. S1B, the absorbance of non-targeted ELR polymers (Control and Akt-in) was almost 0, whereas targeted polymers (tControl and tAkt-in) showed absorbance values of around 0.6, thereby confirming the conjugation of the DNA aptamer to ELR polymers.

3.3. Effect of CD44 targeting in *in vitro* assays

The effect of the CD44 aptamer was determined in human colorectal

cancer and endothelial cells incubated with previously described self-assembled ELR-based nanoparticles carrying an Akt inhibitor [21,22], with the DNA aptamer anchored to the corona (Control and Akt-in tNPs), or lacking the targeting system (Control and Akt-in NPs).

Control nanoparticles, with (Control tNPs) or without the targeting system (Control NPs), did not affect cell proliferation in either Caco-2 or HUVEC cells (Fig. S2) and the curves fitted the standard growth in cell types [42]. These results demonstrate that the ELR structure does not have a cytotoxic effect even after chemical attachment of the DNA aptamer.

In contrast, proliferation of Caco-2 cells was dramatically affected after treatment with nanoparticles carrying the Akt inhibitor (Akt-in NPs) (Fig. 2A,C). As expected, when incubated with targeted nanoparticles (Akt-in tNPs), Caco-2 proliferation was affected earlier than those cells incubated with the therapeutic nanoparticles lacking the targeting system against CD44 (Akt-in NPs). Thus, the lowest concentration (0.25 mg/mL) of targeted nanoparticles (Akt-in tNPs) was more effective than the highest concentration (1 mg/mL) of untargeted nanoparticles (Akt-in NPs). These results confirmed that the DNA

aptamer against CD44 was effective for nanoparticle internalization in colorectal cancer cells. Moreover, although slightly affected by nanoparticles with the Akt inhibitor at very early time points, HUVEC cells were able to keep proliferating similarly to untreated cells (Fig. 2B,D). This effect was independent of the presence of the targeting system and was not statistically significant.

As such, we can conclude that chemical linking of the CD44 aptamer to the nanoparticle corona both improves the cytotoxic action of the therapeutic nanodevices in targeted cancer cells and also helped to widen the therapeutic window, thereby decreasing the off-target effect on non-cancer cells.

3.4. Physicochemical characterization of ELR nano hybrids

Although the CD44-targeted nanoparticles showed high cytotoxicity in colorectal cancer cells, we hypothesized that combining Akt inhibition and the chemotherapeutic drug DTX could improve the therapeutic window. Taking advantage of the SAS technique, we have previously successfully encapsulated DTX into ELR nanoparticles for cancer

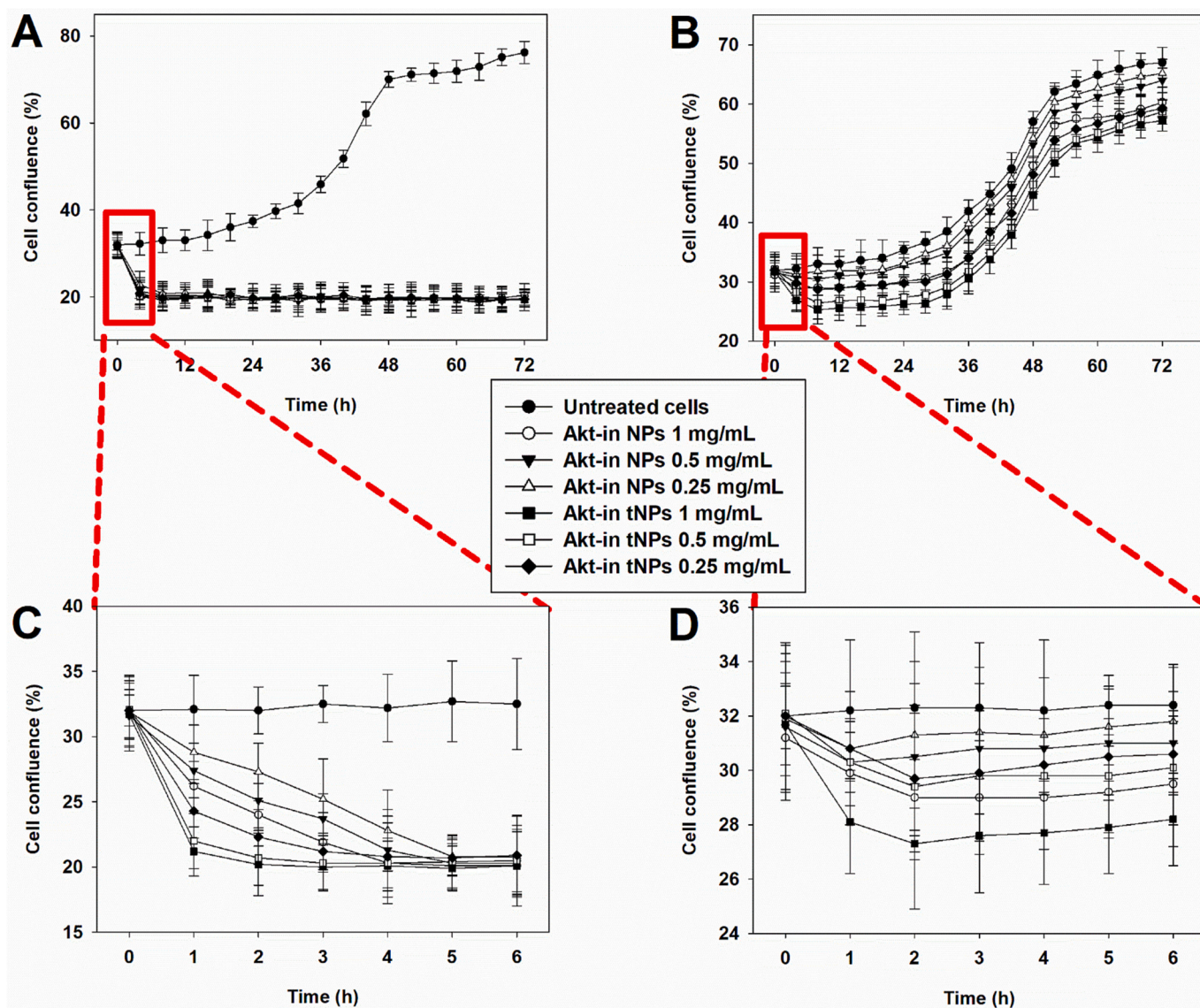


Fig. 2. Effect of targeted ELR nanoparticles carrying the Akt inhibitor on Caco-2 (A and C) and HUVEC (B and D) cell proliferation analyzed by cell confluence measurements. A-B: Cells were incubated with nanoparticles carrying Akt inhibitor for 72 h and confluence was measured using OMNI software. Both untargeted (Akt-in NPs) and targeted (Akt-in tNPs) nanoparticles were used. Confluence percentages were determined every 4 h. C-D: Magnification of the confluence percentages determined each hour during the first 6 h. Three independent experiments were performed, each in triplicate. Mean \pm SD.

therapy. Herein, we synthesized the multicomponent nanohybrids described in Fig. 1 by SAS as a dual-approach drug-delivery system.

Tumors are characterized by hypervascularization, aberrant vascular architecture, high production of vascular permeability factors, and deficient lymphatic drainage [43]. Cancer nanomedicine takes advantage of the enhanced permeability and retention effect (EPR) resulting from this special physiology of tumors to enter and be retained within tumor tissues, thereby showing high accumulation compared to other organs with normal vasculature [43]. Thus, physicochemical properties, (*i.e.*, size, shape, surface charge) are key parameters when designing nanosystems that can reach tumor tissues within the body while avoiding entrapment by the liver and kidneys.

The physicochemical characterization showed that ELR nanohybrid diameters ranged from 52 (tNPs-Ai and tNPs-Ai-DTX) to 67 nm (tNPs-DTX). In addition, all nanohybrid sizes were between 10 and 100 nm, the preferred range when working with nanosystems for drug delivery [10]. Our results also showed low Pdis, thereby suggesting high stability and a low tendency to aggregate, which may interfere with cellular uptake and hinder accurate delivery of DTX and AKT inhibitor inside

cancer cells. The TEM and AFM images also showed spherical nanohybrids (Fig. 3), which makes the entry of these nanosystems into cells easier. The surface charge is particularly important in terms of nano-device stability and electrostatic interactions between nanoparticles and the cell membrane [44]. Our nanohybrids showed a negative ζ -potential due to the presence of glutamic acid residues belonging to the hydrophilic ELR block (VPGE) and DNA aptamer attached to the corona (Table 1). The presence of the CD44 aptamer was confirmed by the diminishment of the ζ -potential in comparison with similar nanoparticles lacking the targeting system previously described by our group [22,31].

After systematic administration, interaction with plasma proteins could affect the fate of the nanohybrid in the bloodstream. Thus, ELR-based nanohybrids were evaluated in a standard *in vitro* plasma protein-binding assay with BSA, as albumin is the major blood protein [45], or FBS. Incubation with BSA, FBS or complete DMEM medium did not show significant changes in terms of particle size over time (Table 1 and Fig. S3), thus allowing us to conclude that ELR nanohybrids remain stable under physiological conditions.

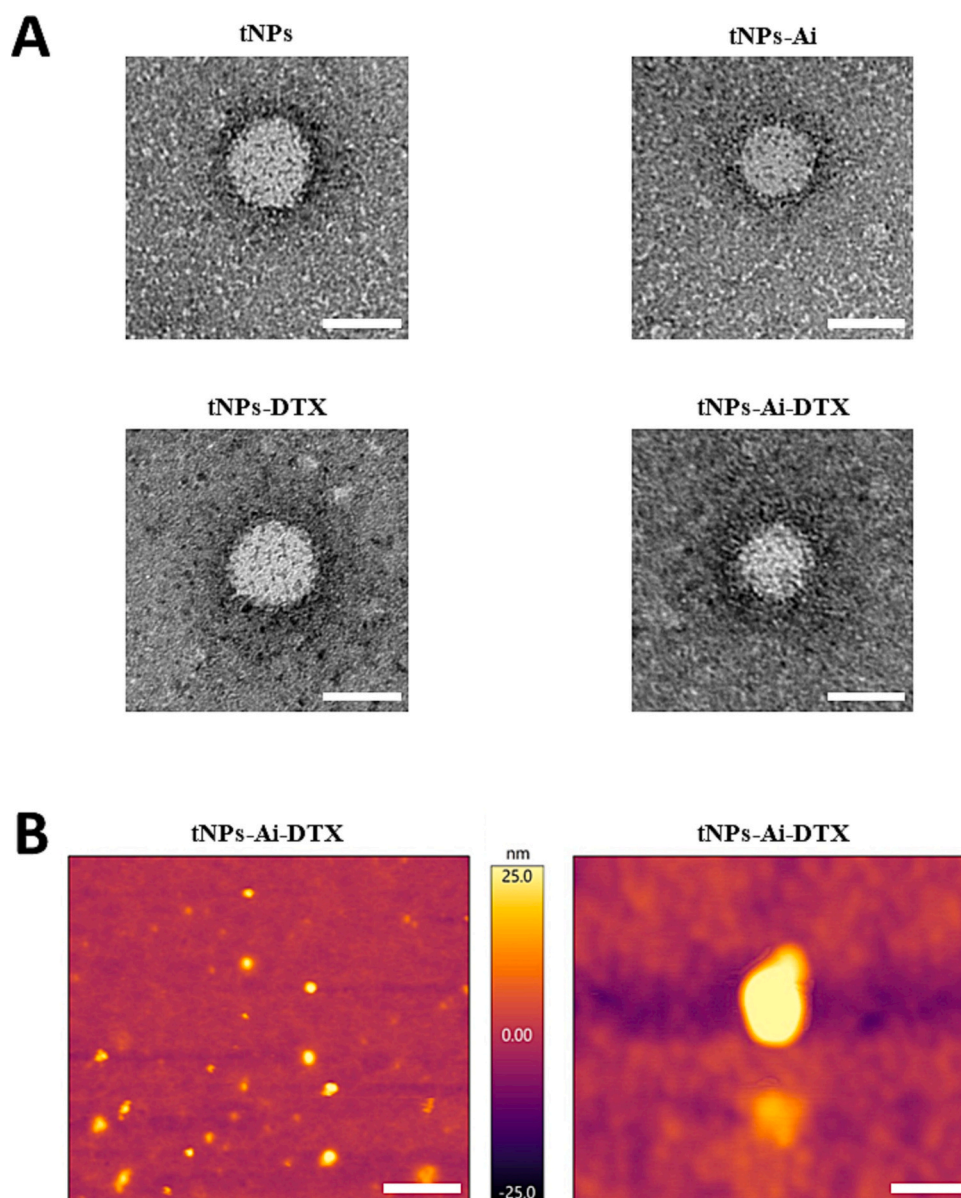


Fig. 3. A: Representative TEM images of ELR nanohybrids. Scale bars: 50 nm, as indicated. B: Representative AFM images of tNPs-Ai-DTX nanohybrids. Scale bars: 50 nm (right) and 500 nm (left).

Table 1

Characterization of ELR nanohybrids. The surface charge of nanohybrids dissolved in 1 mM NaCl ultrapure water type I was measured by electrophoretic light scattering (ELS). The size and polydispersity index (PDI) of nanohybrids dissolved in PBS, PBS + 5 % BSA, FBS or complete DMEM medium were measured by dynamic light scattering (DLS). Mean \pm SD.

| Nanohybrid | ζ -Potential (mV) | PBS | | PBS + 5 % BSA | | FBS | | Complete DMEM | |
|-------------|-------------------------|----------------|-------|----------------|-------|----------------|-------|----------------|-------|
| | | Size (nm) | PdI |
| tNPs | -31.3 \pm 1.3 | 61.5 \pm 2.3 | 0.201 | 62.3 \pm 3.6 | 0.254 | 63.1 \pm 3.1 | 0.269 | 62.5 \pm 2.7 | 0.231 |
| tNPs-Ai | -28.2 \pm 2.2 | 52.1 \pm 3.1 | 0.134 | 51.9 \pm 1.9 | 0.168 | 52.4 \pm 3.2 | 0.234 | 52.2 \pm 2.4 | 0.217 |
| tNPs-DTX | -28.6 \pm 0.4 | 67.5 \pm 1.3 | 0.178 | 68.6 \pm 1.8 | 0.224 | 67.8 \pm 1.9 | 0.231 | 66.9 \pm 2.1 | 0.204 |
| tNPs-Ai-DTX | -26.7 \pm 0.4 | 52.1 \pm 3.3 | 0.176 | 53.4 \pm 2.8 | 0.212 | 52.8 \pm 2.2 | 0.224 | 52.6 \pm 2.6 | 0.206 |

3.5. Drug release study

A kinetic release study was performed by comparing tNPs-DTX and tNPs-Ai-DTX with pure DTX to determine the release kinetics of the encapsulated drug. Fig. 4A shows the percentage of drug released from the tNPs-DTX and tNPs-Ai-DTX nanohybrids.

Thus, 63 % and 56 % of the drug was released from tNPs-DTX and tNPs-Ai-DTX nanohybrids, respectively, in the first 24 h of the experiment, with the release velocity subsequently decreasing until total

release after 168 h. However, 65 % was released from the control sample in the first 2 h and 100 % of DTX was released after 24 h. These results show a clear delay in delivery of the drug from tNPs-DTX and tNPs-Ai-DTX nanohybrids, which is useful for sustained release purposes.

The experimental profile was mathematically fitted using the models described in Section 2.9. Both models fit satisfactorily ($R^2 > 0.980$), with the fit being slightly better for the Peppas-Sahlin equation (Fig. 4B-C). As shown in Table S3, the coefficient n from the Peppas-Sahlin equation has values of between 0.43 and 1, which suggests anomalous transport

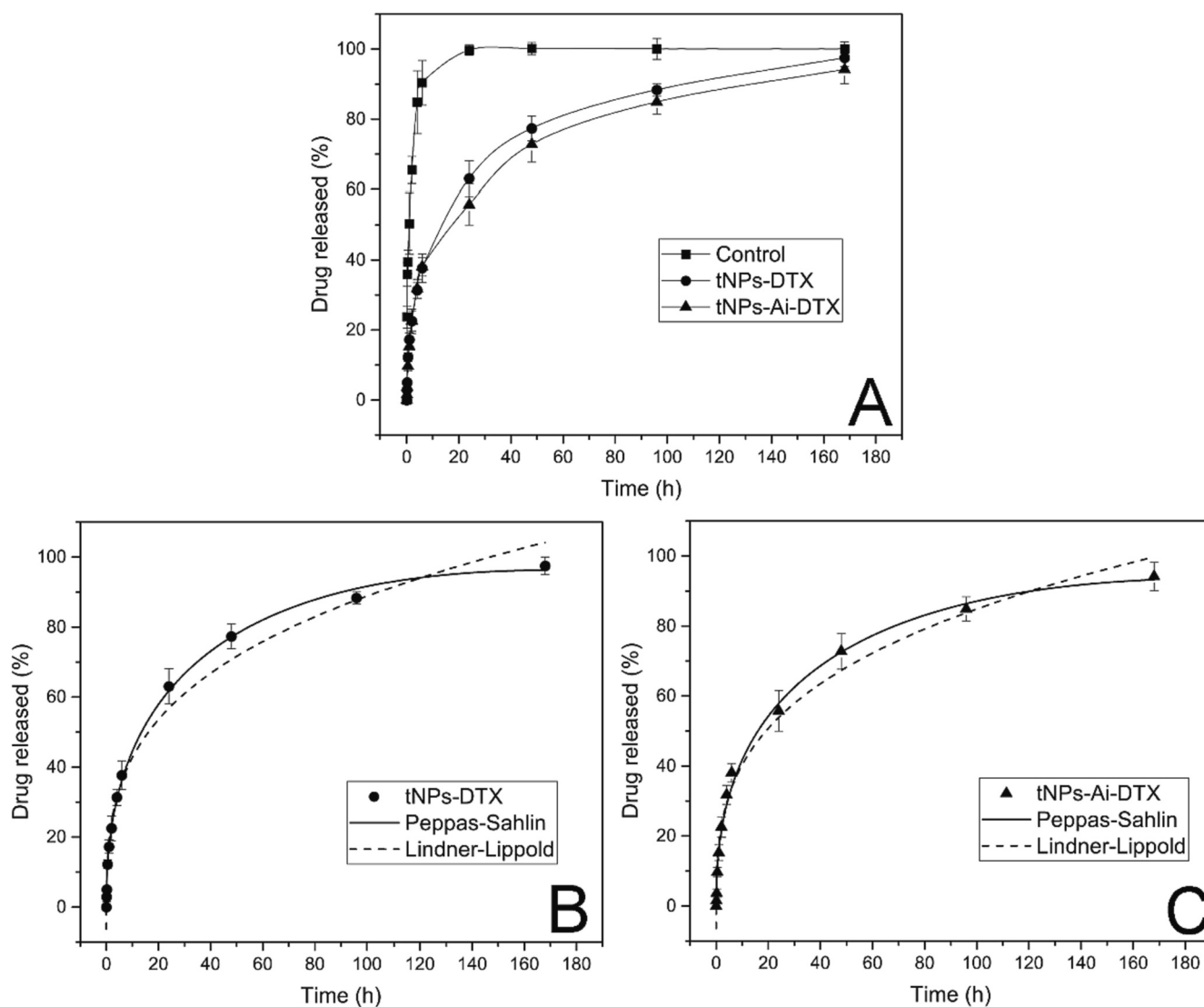


Fig. 4. A: Study of drug release from tNPs-DTX, tNPs-Ai-DTX nanohybrids and free DTX control sample vs. time (h) in PBS release medium at 37 °C at a normalized concentration of 0.06 mg/mL in DTX. Results of the triplicate assay at each time point are presented as Mean \pm SD. ■: Control ● tNPs-DTX ▲: tNPs-Ai-DTX. Lines are used to guide the eye. B: Graphical fitting of the different mathematical models used to describe the release of DTX from tNPs-DTX (●). C: Graphical fitting of the different mathematical models used to describe the release of DTX from tNPs-Ai-DTX (▲). Solid line: Peppas-Sahlin fitting; Dashed line: Lindner-Lippold fitting.

due to the slow rearrangement of polymeric chains and the diffusion process occurring simultaneously, thus resulting in anomalous time-dependent effects. Furthermore, the value of n indicates that the geometry of the nanohybrids in the release medium is spherical, thereby corroborating the results previously obtained by TEM and AFM.

Further analysis of the results obtained when fitting the release profiles indicated that the k_1 parameter representing Fick diffusion was predominant in the Peppas-Sahlín model, with some negative influence of the k_2 term corresponding to the relaxation of the polymeric chains, thereby confirming that the mechanism of drug release was anomalous transport. These results are in agreement with those reported in the literature for similar ELR structures [31].

Fitting of the release profiles to the Lindner-Lippold equation showed that the parameter b (burst effect) was negative or close to zero in both cases, thus indicating that DTX was released from the nanohybrid core and the amount present on the surface was negligible.

3.6. Effect of ELR nanohybrids on cell proliferation

The effect of the dual-approach ELR nanohybrids on cell proliferation was determined *in vitro* in colorectal cancer Caco-2 cells and endothelial HUVEC cells (Figs. 5, S4 and S5).

Control ELR nanohybrids comprising only the amphiphilic ELR backbone and the targeting system with no therapeutic agents (tNPs) were innocuous for both the colorectal cancer and non-cancer cells because their cell proliferation curves fitted with the standard growth in these kinds of cells (Fig. 2) [42]. In contrast, our results showed that cell proliferation of colorectal cancer cells treated with 1 μM free DTX stopped after 12 h (Figs. 5A,C and S4). This effect was also observed after incubation with the same concentration of encapsulated DTX (tNPs-DTX). However, ELR nanohybrids carrying only the Akt inhibitor (tNPs-Ai) affected cell proliferation at an earlier stage. This fast effect on cell proliferation was also observed when cancer cells were incubated with dual-approach nanohybrids carrying both Akt inhibitor and DTX (tNPs-Ai-DTX). Thus, the results showed that the effect of the Akt inhibitor was faster than that observed with the chemotherapeutic agent

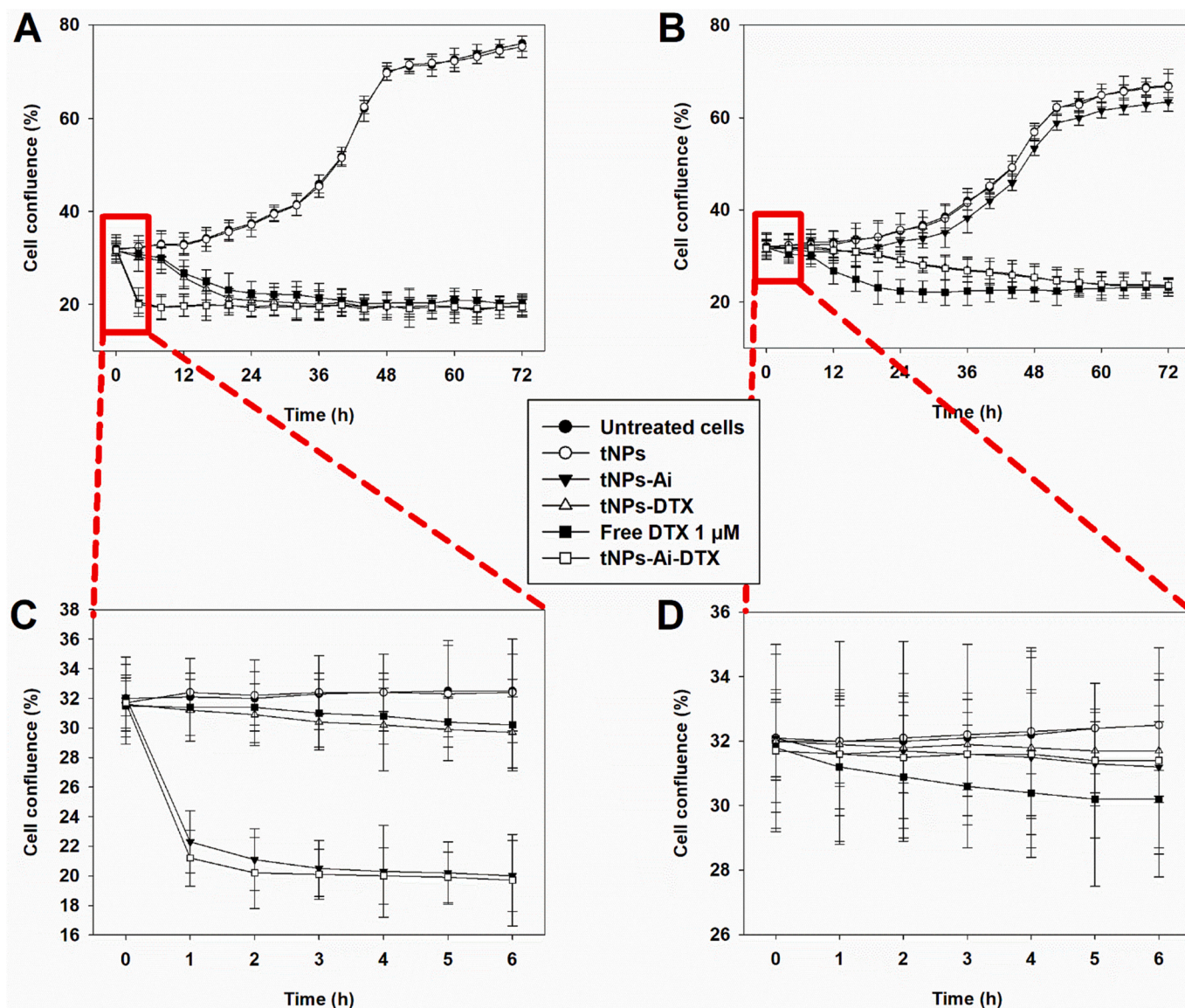


Fig. 5. Effect of ELR nanohybrids on Caco-2 (A and C) and HUVEC (B and D) cell proliferation analyzed by cell confluence measurements. A-B: Cells were incubated with free DTX or ELR nanohybrids for 72 h and confluence was measured using OMNI software. Confluence percentages were determined every 4 h. C-D: Magnification of the confluence percentages determined each hour during the first 6 h. Three independent experiments were performed, each in triplicate. Mean \pm SD.

DTX.

When endothelial cells were treated with tNPs, cell proliferation was not affected and the results were similar to those for untreated cells (Figs. 5B,D and S5). In addition, nanohybrids carrying only Akt inhibitor (tNPs-Ai) affected cell proliferation only slightly. This result can be explained by the fact that only a limited number of nanohybrids is able to enter the endothelial cells compared to cancer cells, which over-express CD44 and therefore exhibit enhanced nanohybrid internalization. Thus, this result demonstrated the desired action of the cancer specific CD44 targeting system. In contrast, free DTX markedly affected cell proliferation of non-cancer cells, which confirmed the main problem inherent to most chemotherapeutic agents currently used, namely that their effect is not selective for cancer cells. Since the mechanism of action of DTX is based on an antimitotic effect due to tubule polymerization, the drug has an enhanced effect in cancer cells as a result of their aberrant cell division rate, although it also has off-target effects in healthy tissues.

Encapsulated DTX (tNPs-DTX) affected cell proliferation in endothelial cells since, although targeted nanohybrids were not internalized in non-cancer cells, DTX was released into the culture medium at the speed shown in Fig. 4 and, as a consequence, the antimitotic drug had an effect. These results, together with the *in vitro* drug delivery, show that nanohybrids meet the requirements for effective drug delivery since these nanoparticles reach the desired sites after administration and act only on target cells, with no harmful effects on healthy tissue [46]. Furthermore, the desired action of the CD44 aptamer can be seen when comparing the effect of ELR nanohybrids on the proliferation of Caco-2 (Figs. 5A,C and S4) and HUVEC cells (Figs. 5B,D and S5). Thus, when incubated with either tNPs-DTX or tNPs-Ai-DTX, cell proliferation was altered at earlier time points in colorectal cancer cells. Finally, when HUVEC cells were incubated with combined therapy using dual nanohybrids (tNPs-Ai-DTX), the effect on cell proliferation was similar to that observed in cells treated with tNPs-DTX. Together, these results confirm that incorporation of the DNA aptamer specifically targeting the CD44 cancer marker enhances the internalization of the nanohybrids by colorectal cancer cells.

We can therefore conclude that colorectal cancer cells are unable to proliferate after treatment with ELR nanohybrids combining both Akt inhibitor and DTX. Moreover, the therapeutic action of the dual-approach system was faster than nanohybrids containing only encapsulated DTX.

3.7. Specific cytotoxicity of ELR nanohybrids

Once the influence of ELR nanohybrids on cell proliferation had been determined, their specific cytotoxicity was studied in colorectal cancer and endothelial cells (Fig. 6A). Two different incubation times (30 min and 24 h) were used based on the proliferation assays described above and previous studies regarding time-related drug efficacy, which suggested that the effect of Akt inhibitor was much faster than that attributable to the chemotherapeutic drug DTX.

The initial results showed that control empty nanohybrids (tNPs) did not affect either Caco-2 or HUVEC viability after either short or prolonged incubation times. In contrast, when Caco-2 cells were incubated with nanohybrids carrying only Akt inhibitor (tNPs-Ai), cell viability decreased to 34.8 % and 2.1 % after incubation for 30 min and 24 h, respectively (Fig. 6A). These results corroborated the fast internalization of nanohybrids due to the presence of the CD44 aptamer. The cell viability decreased to 89.2 % and 8.7 % after incubation with DTX-loaded nanohybrids (tNPs-DTX) for 30 min and 24 h, respectively. As such, DTX encapsulation within ELR nanohybrids improved the cytotoxic effect in colorectal cancer cells, as free DTX only decreased cell viability to 94.3 % and 32.1 % after 30 min and 24 h, respectively. These results also corroborated the desired internalization of DTX due to the CD44-driven targeting. Interestingly, the combination of Akt inhibitor and DTX within the same nanohybrid (tNPs-Ai-DTX) seemed to have a

strong effect and the cell viability of Caco-2 decreased to 29.8 % and 2.5 % after 30 min and 24 h, respectively. Moreover, the effect of dual nanohybrids combining both therapeutic agents was statistically significant compared to nanohybrids only carrying Akt-in or encapsulated DTX. Thus, our results demonstrated that the combination of Akt inhibitor and DTX has an enhanced effect in colorectal cancer cells. Furthermore, we can speculate that both therapeutic agents act via different pathways as they exhibit very different incubation times.

With regard to the *in vitro* cytotoxicity in non-tumor cells, nanohybrids provoked completely different effects in HUVEC compared to cancer cells. Thus, all treatments, namely tNPs-Ai, tNPs-DTX, free DTX and tNPs-Ai-DTX, had a minimum effect after incubation for 30 min. However, free DTX markedly affected HUVEC cell viability after long incubation times (24 h), reducing it to 32.8 %. This effect was similar to the result observed in Caco-2 cells, which corroborates the lack of specificity of DTX [25,31,47]. In contrast to results obtained from colorectal cancer cells, DTX encapsulation in CD44 targeted tNPs-DTX nanohybrids reduced the cytotoxicity in non-tumor cells (8.7 % vs. 52.2 %). This result can be explained by DTX release into the culture medium. Interestingly, the viability in HUVEC was only slightly affected after incubation with tNPs-Ai (83.7 %) and was markedly higher than the results for Caco-2. The same effect was observed in dual-approach nanohybrids tNPs-Ai-DTX. This difference suggests the desired action of CD44 aptamer attached to the nanohybrids surface. Taken together, these results showed that dual-approach nanohybrids trigger selective cytotoxicity for colorectal cancer cells, with minor effects in non-tumor ones.

3.8. Cell-death pathway triggered by ELR nanohybrids

As both *in vitro* cell proliferation and viability assays showed that Akt-in and DTX exhibited different temporal therapeutic trends, we hypothesized that this could be explained by the fact that the two therapeutic agents triggered different cell-death pathways. We had previously demonstrated that ELR-based nanoparticles carrying Akt inhibitor trigger apoptosis-mediated cell death as the peptide inhibitor unlocks the signaling pathway blocked by Akt kinase [21,22]. In contrast, DTX provokes both apoptosis and necrotic cell death [48–50]. As such, Caco-2 and HUVEC cells were incubated with therapeutic ELR nanohybrids and the percentages of apoptotic/necrotic cells were analyzed (Fig. 6B). At early time points, after incubation with nanohybrids carrying Akt-in (tNPs-Ai), 95 % and 98 % of Caco-2 and HUVEC cells, respectively, died by apoptosis. However, treatment with either free DTX or encapsulated DTX (tNPs-DTX) for 30 min resulted in both types of cell death (60 % apoptosis and 40 % necrosis for Caco-2; 58 % apoptosis and 42 % necrosis for HUVEC). Moreover, short incubation of Caco-2 cells with dual nanohybrids (tNPs-Ai-DTX) triggered 81 % apoptosis and 19 % necrosis, with similar percentages being observed for HUVEC cultures (85 % apoptosis and 15 % necrosis).

In contrast, 93 % and 97 % of dead colorectal cancer and HUVEC cells, respectively, corresponded to necrotic cells when incubated with nanohybrids carrying only Akt-in (tNPs-Ai) for 24 h. Again, incubation with free DTX or encapsulated DTX (tNPs-DTX) for 24 h resulted in both apoptotic and necrotic Caco-2 cells (55–58 % and 45–42 % respectively). Moreover, incubation of Caco-2 cells with combined Akt inhibitor and DTX (tNPs-Ai-DTX) resulted in 97 % of necrotic cells. Similar results were found when using HUVEC, thus meaning that both therapeutic agents (Akt-in and DTX) have the same molecular mechanism and trigger the same pathways in cancer and non-cancer cells. The change between incubation for 30 min and 24 h could have two different explanations: an early apoptotic state evolving to necrosis and cells that survived Akt-in undergoing necrosis triggered by DTX. As such, we can conclude that, as assumed, the dual-approach nanohybrids tNPs-Ai-DTX may represent two different therapeutic strategies involving two different approaches to treating colorectal cancer cells, namely apoptotic Akt inhibitor and DTX, which also triggers cell necrosis.

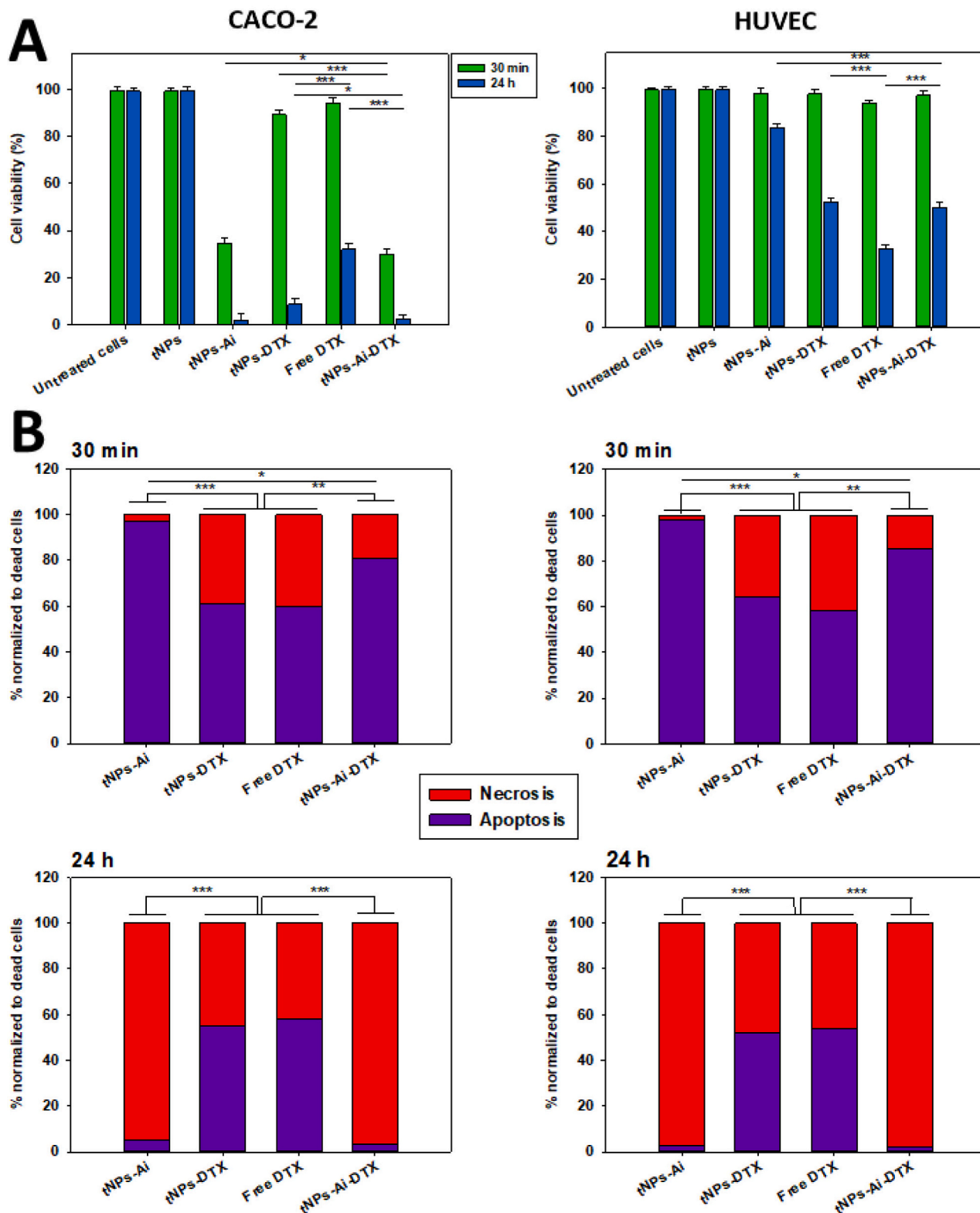


Fig. 6. A: Viability of Caco-2 (left panel) or HUVEC (right panel) incubated with ELR nanohybrids. Cells were incubated with 1 μ M free DTX or ELR nanohybrids at the corresponding normalized concentrations for 30 min (green bars) or 24 h (blue bars) and viability was measured using the LIVE/DEAD Assay. B: Cell-death pathways triggered by ELR nanohybrids in Caco-2 (left panels) or HUVEC (right panels). Cells were incubated with 1 μ M free DTX or nanohybrids at the corresponding normalized concentrations for 30 min (top panels) or 24 h (bottom panels) and an apoptosis (violet)/necrosis (red) assay was performed. Three independent experiments were performed, each in triplicate. Mean \pm SD. * $p < 0.05$, ** $p < 0.01$, *** $p < 0.001$. (For interpretation of the references to colour in this figure legend, the reader is referred to the web version of this article.)

The morphological changes after cell incubation with ELR nano-hybrids were examined by confocal microscopy. For this purpose, a novel ELR nano-hybrid was developed using the SAS technique and rhodamine was encapsulated inside the nano-hybrid core (tNPs-Ai-DTX-Rho). As shown in Fig. 7, rhodamine-loaded nano-hybrids showed perinuclear localization, and typical morphological changes associated with cell death, such as chromatin fragmentation or appearance of apoptotic vesicles, can be seen.

3.9. *In vivo* pharmacokinetic profile

To achieve antitumor efficacy, drug molecules must overcome numerous biological barriers in the human body at the systemic, tissue, cellular and subcellular level between their site of administration and the tumor site [51]. As such, circulating half-life is one of the main features to take into account when designing a novel therapeutic drug [52]. ELRs have been previously shown to be useful tool for extending the *in vivo* circulating half-life of drugs [53,54].

The *in vivo* pharmacokinetic profile was determined by systemic injection of rhodamine-loaded nano-hybrids (tNPs-Ai-DTX-Rho) in BALB/c mice *via* the tail vein. tNPs-Ai-DTX-Rho was used due to the fact that this targeted nano-hybrid contains the dual-approach drug-delivery system. The results showed a single-phase decay behavior of fluorescent nano-hybrids in the plasma, therefore the one-compartmental model was used and the plasma concentration-time curve was fit (Fig. S6). In this model, the whole body is thought to act as a single, uniform compartment and the drug is distributed immediately [55].

The distribution volume and half-life are key pharmacokinetic parameters and, as such, are considered key properties when designing

drug-delivery systems [55]. Our results showed that the distribution volume of ELR nano-hybrids was similar to the theoretical plasma volume in mice (Table 2), thus indicating that they do not accumulate quickly in organs after systemic administration. Moreover, the nano-hybrids showed a long circulating half-life (5.5 h), which was in agreement with previous studies involving ELR nanoparticles developed as drug-delivery systems [54]. Thus, no changes between tNPs-Ai-DTX-Rho and the other nano-hybrids should be expected since there are no differences in their physicochemical features, as described previously. We can conclude that the nano-hybrids developed herein exhibited the required *in vivo* behavior for controlled release of therapeutic agents.

Table 2

In vivo pharmacokinetic parameters for rhodamine-loaded nano-hybrids (tNPs-Ai-DTX-Rho) administered systemically to BALB/c mice *via* the tail vein. Single-compartment analysis. Mean \pm SD. Abbreviations: AUC: Area under the curve; F: Bioavailability; CL: Clearance; Vd: Volume of distribution; $T_{1/2}$ elimination: Terminal half-life; $K_{\text{elimination}}$: elimination rate constant.

| | |
|--|-----------------|
| AUC ($\mu\text{M}\cdot\text{h}$) | 137 \pm 9 |
| F (%) | 100 |
| CL (mL·h) | 0.23 \pm 0.07 |
| Vd (mL) | 1.8 \pm 0.6 |
| $T_{1/2}$ elimination (h) | 5.5 \pm 0.7 |
| $K_{\text{elimination}}$ (h^{-1}) | 0.15 \pm 0.03 |

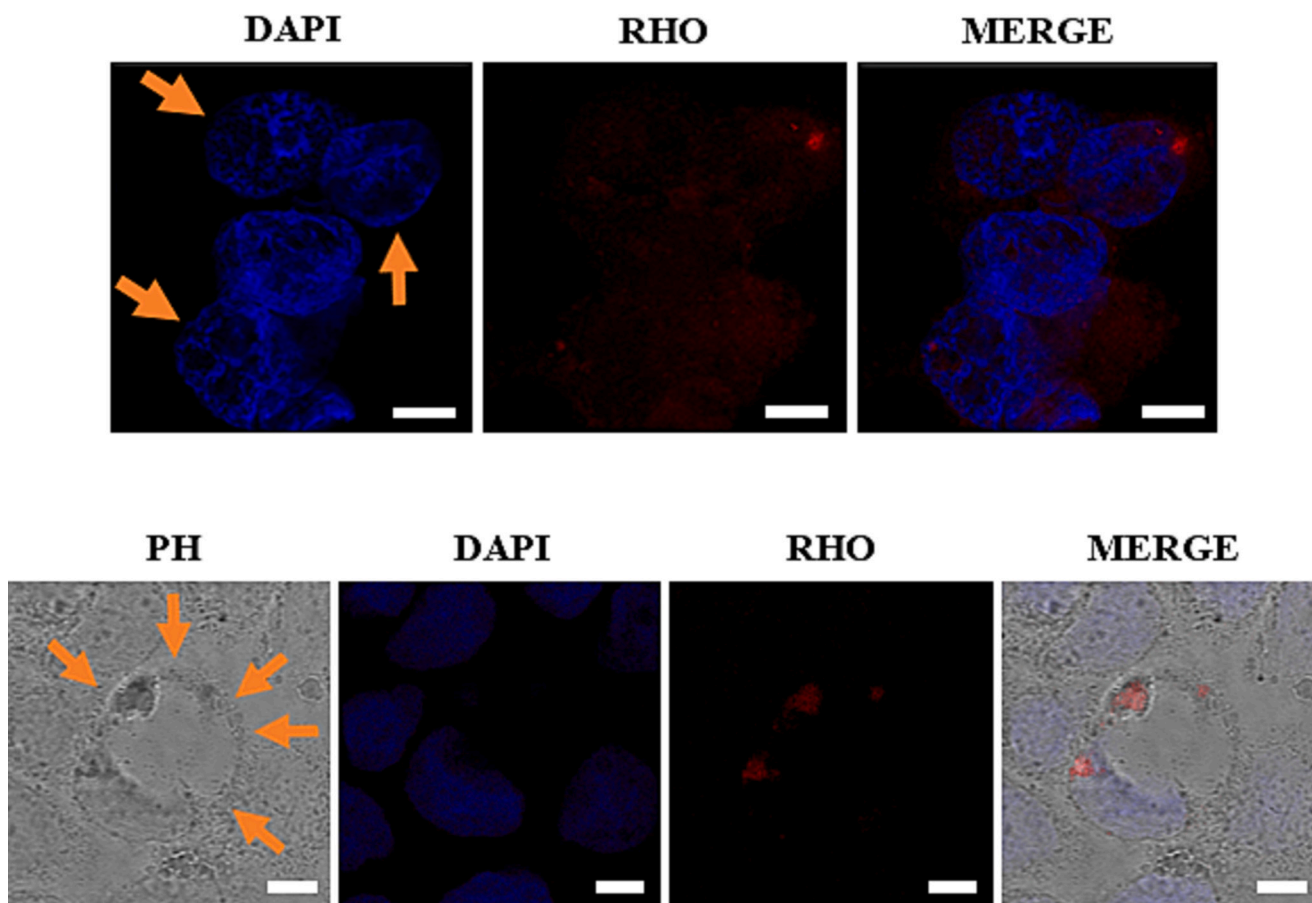


Fig. 7. Representative confocal microscopy images of Caco-2 cells incubated with rhodamine-loaded nano-hybrids. Cells were incubated with tNPs-Ai-DTX-Rho ELR nano-hybrids for 1 h. Fluorescence-field (DAPI and Rhodamine), phase-contrast and merged images. Orange arrows indicate chromatin fragmentation (row 1) and apoptotic vesicle (row 2). Scale bars: 20 μm (rows 1–3) and 10 μm (rows 4–6).

3.10. In vivo anti-cancer efficacy of ELR nanohybrids

In order to determine the efficacy of ELR nanohybrids in colorectal cancer, the azoxymethane/dextran sodium sulfate (AOM/DSS) murine model was used [32]. AOM-induced tumors exhibit molecular and histopathological features similar to human CRC and are usually present in the distal part of the colon, thereby resembling the predominant localization of spontaneous CRC in humans [32]. This animal model has been described as a reliable protocol that exhibits predictable tumor development, as characterized by a high incidence and low mortality in a short-term period [56]. The scheme used for tumor induction in mice is depicted in Fig. 8A. Briefly, the tumorigenic agent azoxymethane (AOM)

was injected intraperitoneally and, after 5 days, the pro-inflammatory agent dextran sodium sulfate (DSS) was provided in drinking water for 5 days, followed by 15 days of regular drinking water. DSS treatment was repeated twice (total of 3 cycles).

CRC is usually diagnosed on the basis of clinical characteristics and endoscopic mucosal features. Although colonoscopy allows direct visualization of the colonic mucosa, this technique is invasive and can cause complications, such as bleeding and perforation. Alternatively, the use of non-invasive imaging techniques, including magnetic resonance imaging (MRI), allows monitoring of the disease during its early stages as well as characterization of the disease in more advanced stages [57].

MRI was performed to evaluate the inflammation-driven

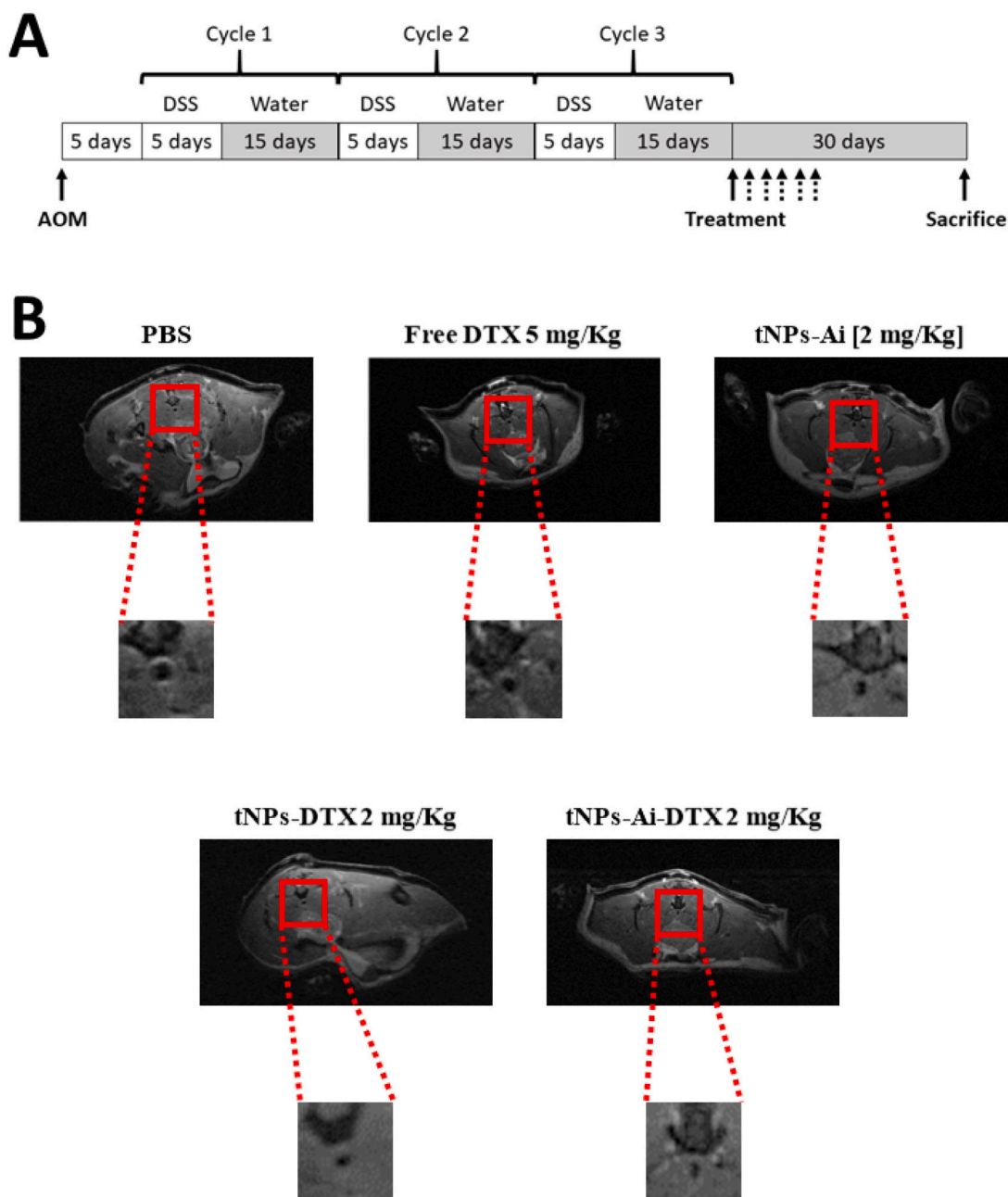


Fig. 8. A: Scheme showing the experimental progress of AOM-induced colon carcinogenesis with inflammation-driven tumor progression. Dashed lines indicate the alternative additional doses of treatment. AOM: Azoxymethane; DSS: Dextran sodium sulfate; Adapted from Neufert et al. [32]. B: Representative MRI images from treated mice. Tumors were induced with AOM/DSS as described in panel A and then mice were injected systemically with different treatments. MRI was performed at day 25 post-treatment. Red arrows indicate the colon. The light halo surrounding the colon indicates inflammation. (For interpretation of the references to colour in this figure legend, the reader is referred to the web version of this article.)

tumorigenesis within the colorectal tract. The lack of water in the colon of healthy mice resulted in a dark image (Fig. S7A), whereas the colonic inflammation triggered by DSS treatment was observed as a brighter halo around the lumen (Fig. S7B, red arrows), thereby corroborating the

characteristic inflammation in the AOM/DSS mouse model by MRI.

As expected, *ex vivo* examination of murine colons showed that control animals did not exhibit visible tumor polyps (Fig. S7C), whereas AOM/DSS treatment provoked tumorigenesis in the murine distal colon,

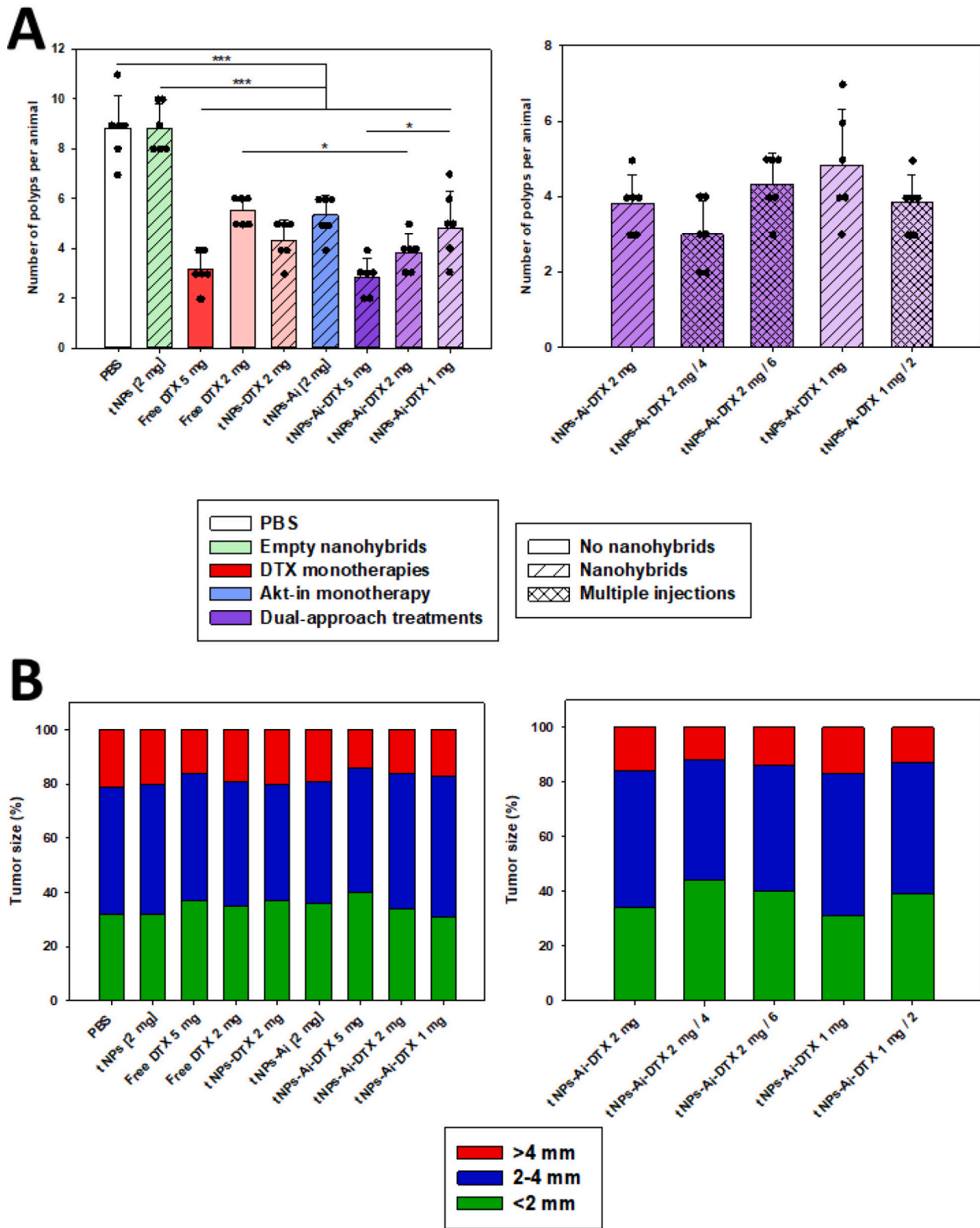


Fig. 9. A: Number of polyps per animal. Each dot depicts one animal. Bars legend: empty: non nano hybrids treatments; striped bars: single injection treatments; squared bars: multiple injections treatments. Colour legend: white: PBS; green: empty nano hybrids; red: DTX monotherapies; blue: Akt-in monotherapy; Violet: dual approach treatments. Mean ± SD. **p* < 0.05, ****p* < 0.001 B: Tumor size distribution. Small (<2 mm), medium (2–4 mm) and large tumor polyps (>4 mm). (For interpretation of the references to colour in this figure legend, the reader is referred to the web version of this article.)

where multiple tumor polyps were detected (Fig. S7D).

A total of 72 mice ($n = 6$ for each treatment) were used for tumor induction and, at the end of the protocol, these animals were divided randomly into 12 experimental groups (Table S4). A placebo group (mice treated with PBS) and a control group treated with empty nanohybrids (tNPs [2 mg]) were included as negative controls. Since there is no standard dose of DTX for *in vivo* assays in the literature and the drug dose varies widely [26–28,58,59], two different quantities of DTX were included in the *in vivo* assays: 2 and 5 mg/kg. As such, we established two experimental groups involving free DTX: free DTX 5 mg/kg and free DTX 2 mg/kg. Furthermore, a further two groups were included as control of treatment with a single therapeutic agent: nanohybrids containing only DTX 2 mg/kg (tNPs-DTX 2 mg) and nanohybrids containing only Akt inhibitor (tNPs-Ai [2 mg]). The use of brackets in tNPs [2 mg/kg] and tNPs-Ai [2 mg/kg] group names means that these groups were administrated with the same amount of ELR as the tNPs-DTX 2 mg/kg group. The same amounts of the encapsulated chemotherapeutic drug DTX were used for the groups receiving dual-approach ELRs: tNPs-Ai-DTX 5 mg/kg and tNPs-Ai-DTX 2 mg/kg. Moreover, we used a third dose of 1 mg DTX/Kg (tNPs-Ai-DTX 1 mg/kg) in order to achieve the minimum dose able to trigger an effective therapeutic effect. Apart from the efficacy of ELR nanohybrids as anti-cancer treatment, the posology was also determined to study the effect of multiple administrations instead of one single injection with the same amount of drug with the aim of improving the therapeutic activity of the nanohybrids. Moreover, this multidose strategy could be an encouraging approach to avoid side effects of the chemotherapeutic agent DTX. For these reasons, three multidose groups (administrations every 3 days) were included in the *in vivo* assay: tNPs-Ai-DTX 1 mg/kg /2 (2 injections, 0.5 mg/kg each injection, 1 mg/kg in total), tNPs-Ai-DTX 2 mg/kg /4 (4 injections, 0.5 mg/kg each injection, 2 mg/kg in total) and tNPs-Ai-DTX 2 mg/kg/6 (6 injections, 0.33 mg/kg each injection, 2 mg/kg in total).

Body weight and animal welfare were monitored during the whole assay (Fig. S8). The results showed that untreated animals (PBS group) and those treated with control empty nanohybrids (tNPs [2 mg/kg]) showed a loss of body weight, whereas mice treated with ELR nanohybrids remained healthy and maintained a stable body weight.

As explained above, our nanohybrids met the requirements for systemic administration as they were not affected by interaction with BSA plasma protein and showed a good pharmacokinetic profile. As such, these nanohybrids were administrated systemically by intravenous injection *via* the tail vein in mice. As no macroscopic examination was possible without animal sacrifice, MRI was performed 25 days post-injection to obtain preliminary results in terms of the efficacy of ELR-based nanohybrids for resolving inflammation-driven carcinogenesis (Fig. 8B). The MRI results showed that mice treated with tNPs-DTX-Ai 2 mg/kg presented less inflammation than untreated mice (PBS group). Moreover, both tNPs-Ai [2 mg/kg] and tNPs-DTX 2 mg/kg seemed to resolve inflammation better than free DTX, in which inflammation (indicated by the bright halo) was better appreciated (Fig. 8B).

Ex vivo examination of murine colons at the end of the treatment revealed significant differences between the groups in terms of the number of tumor polyps per animal (Fig. 9A). Thus, untreated animals (PBS group) had 8.83 tumor polyps on average and similar values were found in mice treated with empty ELR nanohybrids (tNPs [2 mg/kg]). The examination of colons from animals treated with anti-tumor devices showed a significant decrease in terms of the number of tumors per animal, with the groups treated with 5 mg/kg or 2 mg/kg free DTX presenting 3.17 and 5.5 tumors per animal on average, respectively, thereby indicating that administration of free DTX had a dose-dependent effect on the number of polyps. Moreover, when DTX was encapsulated within targeted nanohybrids (tNPs-DTX 2 mg/kg), the number of tumor polyps diminished to 4.33. As such, encapsulation of the chemotherapeutic drug enhanced its anti-cancer effect. This result can be explained by the higher bioavailability of the drug due to encapsulation and by the efficiency of the targeting system against CD44 in cancer cells.

Nanohybrids carrying only Akt inhibitor (tNPs-Ai [2 mg/kg]) also reduced the number of tumor polyps (5.33 tumors) to a similar extent as free DTX (5.5 tumors), despite triggering a more complex therapeutic mechanism. Although previous results from our group had highlighted the encouraging therapeutic activity of ELR-based nanoparticles involving Akt kinase [21,22], this is the first time that controlled release of this Akt inhibitor leads to tumor reduction *in vivo*.

As regards the combination of Akt inhibition and DTX within the same nanohybrid (tNPs-Ai-DTX), a dose-dependent effect was observed and animals only presented 2.83, 3.83 and 4.83 polyps, on average, when treated with dual-approach nanohybrids (5, 2 and 1 mg/kg of DTX, respectively). These results therefore show the enhanced effect of the Akt inhibitor and DTX when included within the same vehicle, since the combined therapy improves both the therapeutic action of free DTX and that of the nanohybrids containing only one therapeutic agent.

To determine the dose regime for the nanohybrid therapy, the effect of multiple administrations (each 3 days) of dual-approach nanohybrids (tNPs-Ai-DTX) on the number of tumor polyps was also studied (Fig. 9A). This strategy may be a promising approach as it could reduce problems related to the administration of DTX and the subsequent adverse side effects. Thus, animals treated with tNPs-Ai-DTX 1 mg/kg in 2 injections presented fewer tumor polyps (3.83 in average) than animals treated with the same quantity of nanohybrids in a single injection (4.83 polyps). Moreover, the enhanced effect from multidose treatment was appreciated in animals treated with tNPs-Ai-DTX 2 mg/kg dosed in four injections compared to animals treated with tNPs-Ai-DTX 2 mg/kg in one systemic injection (3 and 3.83 polyps, respectively). However, this effect was not seen when tNPs-Ai-DTX 2 mg/kg was administrated in six injections, as this group presented 4.33 tumor polyps per animal. Although this group presented a significantly lower number of tumor polyps than the PBS group, the worse anti-tumor activity could be explained by the fact that the effective dose in each administration was not sufficient to improve the results obtained for animals treated with only one administration. Thus, multiple administrations improved the effect of the chemotherapeutic drugs with a minimal dose of 0.5 mg/kg per injection. Considering these results, the best anti-tumor activity in terms of number of tumor polyps was found when treating with free DTX 5 mg/kg, tNPs-Ai-DTX 5 mg/kg or tNPs-Ai-DTX 2 mg/kg dosed in four injections.

Ex vivo examination of murine colons also involved the measurement of tumor polyp size (Fig. 9B and Table S5), with tumor polyps being divided into three different groups: small (<2 mm), medium (2–4 mm) and large (>4 mm). Most tumors from untreated animals (PBS group) had a size of between 2 and 4 mm (45 %), whereas small polyps and large polyps accounted for 32 % and 21 % of the total, respectively (S32/M45/L21 tumor size pattern). Systemic administration of control empty ELR nanohybrids (tNPs [2 mg/kg]) did not change the tumor size distribution. This result, together with the absence of variation in terms of tumor numbers, shows that the ELR backbone does not influence the progress of the disease. Although free DTX had a dose-dependent effect in terms of number of tumor polyps (Fig. 9A), tumor size pattern was not changed.

Neither DTX encapsulation within nanohybrids (tNPs-DTX 2 mg/kg) nor nanohybrids carrying only Akt inhibitor (tNPs-Ai [2 mg/kg]) did not alter the size distribution. Contrary, animals treated with dual-approach nanohybrids showed less large tumors (>4 mm) and more small polyps (<2 mm): S40/M46/L14, S34/M50/L16 and S31/M52/L17 for animals treated with tNPs-Ai-DTX 5 mg/kg, tNPs-Ai-DTX 2 mg/kg and tNPs-Ai-DTX, respectively.

The effect of multiple administrations (every 3 days) of dual-approach nanohybrids (tNPs-Ai-DTX) on the size distribution of tumor polyps was also studied (Fig. 9B and Table S5). The results suggest that animals treated with tNPs-Ai-DTX in two, four or six doses showed that the use of multiple doses of ELR nanohybrids slightly reduced the tumor volume compared to the same amount of drug in a single injection.

Taken together, although our results show that animals treated with

tNPs-Ai-DTX 2 mg/kg / 4 presented the same number of tumor polyps as the animals treated with free DTX 5 mg/kg or tNPs-Ai-DTX 5 mg/kg, the size distribution changed towards smaller tumor polyps in animals from tNPs-Ai-DTX 2 mg/kg/4 group. In view of these results, tNPs-Ai-DTX 2 mg/kg administrated in four injections can be seen to be the most effective dosage. Moreover, we can speculate that this therapeutic approach should be less toxic for patients due to the lower amount of drug administrated with each injection.

3.11. Histopathological examination of murine colon specimens

Once the anti-tumor activity of ELR nanohybrids had been determined, the histopathological examination of murine colons was performed (Fig. 10). Tumor polyps (red arrows) were found to be abnormal solid masses comprising a tumor core surrounded by connective tissue and blood vessels. These regions showed a high cell density, as demonstrated by the more intense haematoxylin staining compared to the rest of the tissue and were compatible with invasive carcinoma.

Histological analysis of both PBS and tNPs [2 mg/kg] groups showed severe crypt damage and high architectural distortion. Cell infiltration was also perceived, most likely as AOM-induced tumors are frequently infiltrated by T lymphocytes and other immune cells [60]. The morphological and pathological features were in agreement with high-grade dysplasia, the previous stage before malignant degeneration and invasion of the bowel wall [61]. Histological sections from animals treated with tNPs-Ai [2 mg/kg] or tNPs-DTX showed unstructured tissue, the gastrointestinal crypts of which had aberrant shapes. However, infiltrating cells were better appreciated in sections from animals treated with tNPs-DTX [2 mg/kg]. With regard to animals treated with tNPs-Ai-DTX 2 mg/kg in a single dose, tissue sections seemed to show mild disruption and higher structuration and organization. Although some abnormal crypts could be seen, most crypts possessed small and round shapes. Furthermore, there were no differences compared to murine colons from animals treated with the same amount of ELR nanohybrids in four administrations (tNPs-Ai-DTX 2 mg/kg/4). Thus, colons from animals treated with dual-approach ELR nanohybrids showed structured tissue with a majority of normal crypts and fewer infiltrating cells.

4. Conclusions

Cancer is a complex disease involving multiple processes, thus making the effective action of a single therapy more difficult to achieve. As such, current therapeutic strategies are based on combinations of different approaches, such as surgery, chemotherapy, radiotherapy, immunotherapy or nanomedicine [62]. In this context, we hypothesized that ELR nanohybrids could be a smart system for combining several therapeutic agents. Thus, we designed and produced hybrid nanoparticles involving Akt inhibition and release of the anti-mitotic drug Docetaxel as a dual-approach drug-delivery strategy specifically targeted to CD44. Indeed, the presence of targeting systems is essential for successful development of cancer therapies, since nanomedicine requires more complex systems that are able to combine as many therapeutic strategies as possible. To the best of our knowledge, this is the first time that nanosystems carrying DTX and an Akt inhibitor simultaneously have been evaluated for therapeutic purposes in CRC.

Both physicochemical characterization and *in vivo* pharmacokinetic assays demonstrated that our ELR nanohybrids exhibit high stability in plasma solution and a long half-life in systemic circulation. Furthermore, *in vitro* assays showed that targeted dual-approach nanohybrids are able to impair colorectal cancer cell proliferation and viability, with minimum cytotoxicity in non-cancer cells. Moreover, our advanced nanosystem was shown to specifically tackle cancer cells *via* two different pathways: the Akt inhibitor provokes apoptosis, whereas DTX triggers both apoptosis- and necrosis-mediated cell death. Furthermore, DNA aptamer-based targeting reduced nonspecific cytotoxicity from DTX and significantly improved the anti-tumor effect of our dual-approach nanosystems compared to AKT inhibition or DTX monotherapies.

The *in vivo* assays in a colorectal cancer mouse model showed that this dual-approach strategy enhances the anti-tumor efficacy compared to Akt or DTX monotherapies. Moreover, our results show that multiple administrations of ELR nanohybrids reduce the number of tumor polyps compared to a single injection with the same amount of therapeutic agent. Furthermore, the histopathological examination of murine colons showed that systemic administration of dual-approach ELR nanohybrids improved tissue organization and gastrointestinal crypt morphology.

In summary, the nanosystem described herein opens up an encouraging strategy for controlled release of combined therapeutic agents. This approach could form the basis for other combined therapeutic strategies against a wide range of solid tumors, since this highly tunable nanosystem can be modified to incorporate a huge variety of cytotoxic drugs and active targeting molecules.

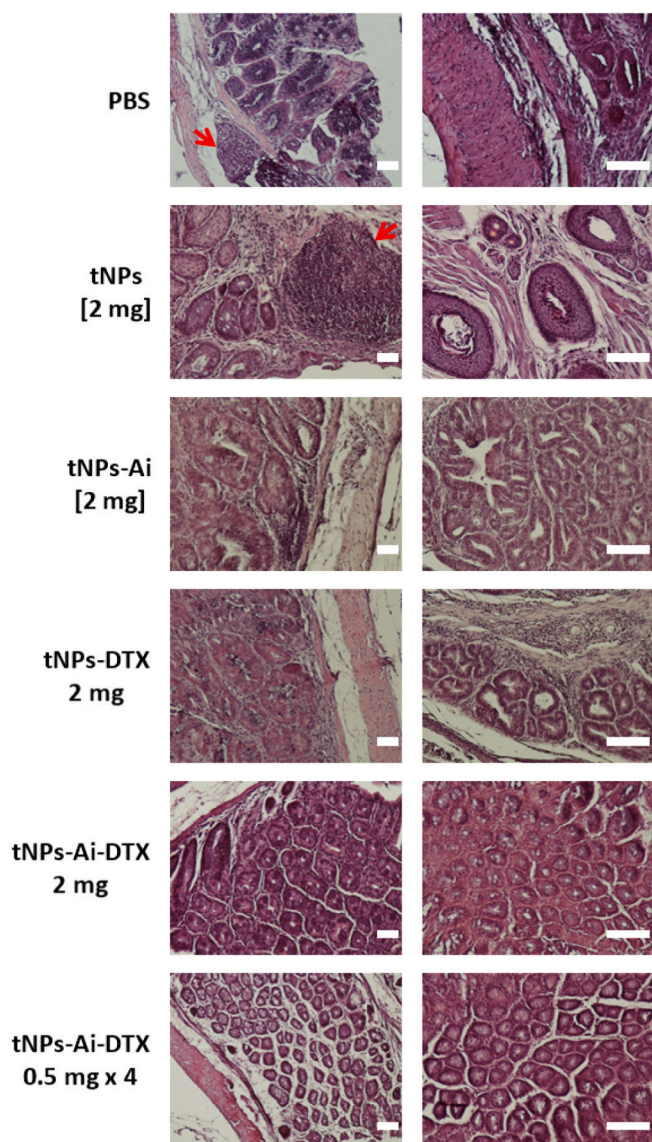


Fig. 10. Histopathological analysis of murine colons after haematoxylin-eosin (H&E) staining: effect of ELR nanohybrids in CRC tumorigenesis in mice. After animal sacrifice, colons were collected and processed for histological evaluation. Representative images of H&E stained sections. Magnification: 10× (left column) and 20× (right column). Scale bars: 200 μm.

CRedit authorship contribution statement

Juan Gonzalez-Valdivieso: Investigation, Methodology, Data curation, Formal analysis, Software, Writing – original draft, Writing – review & editing. **Reinaldo Vallejo:** Investigation, Methodology. **Soraya Rodriguez-Rojo:** Supervision. **Mercedes Santos:** Supervision. **Jose Schneider:** Writing – review & editing. **Francisco Javier Arias:** Conceptualization, Funding acquisition, Supervision, Project administration, Writing – review & editing. **Alessandra Girotti:** Methodology, Supervision, Project administration, Writing – review & editing.

Declaration of competing interest

The authors declare that they have no known competing financial interests or personal relationships that could have appeared to influence the work reported in this paper.

Data availability

Data will be made available on request.

Acknowledgements

The authors are grateful for financial support from the European Social Fund (ESF), the European Regional Development Fund (ERDF) and the MICIUN (DTS19/00162 and PID2019-106386RB-I00). Soraya Rodriguez-Rojo would like to thank the University of Valladolid for her postdoctoral contract. The authors would like to thank R. Garcia and M. Briongos for their technical assistance with polymer bioproduction as well as R. Alvarez-Delgado for her assistance with animal procedures. The authors would also like to thank J. Gutierrez for his assistance with confocal microscopy, AFM and MRI procedures, as well as Dr. A. Frankland for the English revision.

Appendix A. Supplementary data

Amino acid sequences of ELR polymers (Table S1); chemical binding of CD44 DNA aptamer to ELR polymers (Fig. S1); proportion of components measured by ^1H NMR spectroscopy (Table S2); drug release from ELR nanohybrids (Table S3); proliferation assays in Caco-2 and HUVEC cells after incubation with targeted ELR nanoparticles (Fig. S2); stability of ELR nanohybrids over time (Fig. S3); effect of ELR nanohybrids on Caco-2 cells proliferation (Fig. S4); effect of ELR nanohybrids on HUVEC cells proliferation (Fig. S5); pharmacokinetic profile of ELR nanohybrids after systemic administration in BALB/c mice (Fig. S6); MRI and optical microscopy images of tumor induction by AOM/DSS treatment in BALB/c mice (Fig. S7); experimental groups for the *in vivo* assay (Table S4); body weight change along the treatment (Fig. S8); optical microscopy images of murine colorectal tract after treatment (Fig. S9); and tumor size distribution in mice (Table S5).

References

- [1] World Cancer Research Fund, Cancer statistics. <https://www.wcrf.org/dietandcancer/cancer-trends/colorectal-cancer-statistics> (accessed 15 January 2023).
- [2] National Cancer Institute, Cancer statistics. <https://seer.cancer.gov> (accessed 10 January 2023).
- [3] R.L. Siegel, K.D. Miller, S.A. Fedewa, D.J. Ahnen, R.G.S. Meester, A. Barzi, A. Jemal, et al., CA Cancer J. Clin. 67 (2017) 177–193, <https://doi.org/10.3322/caac.21395>.
- [4] M. Navarro, A. Nicolas, A. Ferrandez, A. Lanas, Colorectal cancer population screening programs worldwide in 2016: an update, World J. Gastroenterol. 23 (2017) 3632–3642, <https://doi.org/10.3748/wjg.v23.i20.3632>.
- [5] C.J. Punt, M. Koopman, L. Vermeulen, From tumour heterogeneity to advances in precision treatment of colorectal cancer, Nat. Rev. Clin. Oncol. 14 (2017) 235–246, <https://doi.org/10.1038/nrclinonc.2016.171>.
- [6] S. Managò, C. Tramontano, D. Delle Cave, G. Chianese, G. Zito, L. De Stefano, M. Terracciano, E. Lonardo, A.C. De Luca, I. Rea, SERS quantification of Galunisertib delivery in colorectal cancer cells by plasmonic-assisted diatomite nanoparticles, Small. 17 (2021), e2101711, <https://doi.org/10.1002/sml.202101711>.
- [7] A. Tiwari, S. Saraf, A. Jain, P.K. Panda, A. Verma, S.K. Jain, Basics to advances in nanotherapy of colorectal cancer, Drug Deliv. Transl. Res. 10 (2019) 319–338, <https://doi.org/10.1007/s13346-019-00680-9>.
- [8] C. Tramontano, J.P. Martins, L. De Stefano, M. Kemell, A. Correia, M. Terracciano, N. Borbone, I. Rea, H.A. Santos, Microfluidic-assisted production of gastro-resistant active-targeted diatomite nanoparticles for the local release of Galunisertib in metastatic colorectal cancer cells, Adv. Healthc. Mater. 12 (2023), e2202672, <https://doi.org/10.1002/adhm.202202672>.
- [9] R. Muñoz, A. Girotti, D. Hileeto, F.J. Arias, Metronomic anti-cancer therapy: a multimodal therapy governed by the tumor microenvironment, Cancers. 13 (2021), <https://doi.org/10.3390/cancers13215414>.
- [10] J. Shi, P.W. Kantoff, R. Wooster, O.C. Farokhzad, Cancer nanomedicine: progress, challenges and opportunities, Nat. Rev. Cancer 17 (2017) 20–37, <https://doi.org/10.1038/nrc.2016.108>.
- [11] J.S. Ryu, D. Raucher, Elastin-like polypeptide for improved drug delivery for anticancer therapy: preclinical studies and future applications, Expert Opin. Drug Deliv. 12 (2015) 653–667, <https://doi.org/10.1517/17425247.2015.974546>.
- [12] S.R. MacEwan, A. Chilkoti, Elastin-like polypeptides: biomedical applications of tunable biopolymers, Biopolymers. 94 (2010) 60–77, <https://doi.org/10.1002/bip.21327>.
- [13] J.C. Rodriguez-Cabello, F.J. Arias, M.A. Rodrigo, A. Girotti, Elastin-like polypeptides in drug delivery, Adv. Drug Deliv. Rev. 97 (2016) 85–100, <https://doi.org/10.1016/j.addr.2015.12.007>.
- [14] E.M. MASTRIA, M. Chen, J.R. McDaniel, X. Li, J. Hyun, M.W. Dewhirst, A. Chilkoti, Doxorubicin-conjugated polypeptide nanoparticles inhibit metastasis in two murine models of carcinoma, J. Control. Release 208 (2015) 52–58, <https://doi.org/10.1016/j.jconrel.2015.01.033>.
- [15] J.R. McDaniel, D.J. Callahan, A. Chilkoti, Drug delivery to solid tumors by elastin-like polypeptides, Adv. Drug Deliv. Rev. 62 (2010) 1456–1467, <https://doi.org/10.1016/j.addr.2010.05.004>.
- [16] D.F. Duarte Campos, C.D. Lindsay, J.G. Roth, B.L. LeSavage, A.J. Seymour, B. A. Krajina, R. Ribeiro, P.F. Costa, A. Blaese, S.C. Heilshorn, Bioprinting cell- and spheroid-laden protein-engineered hydrogels as tissue-on-chip platforms, Front. Bioeng. Biotechnol. 8 (2020) 374, <https://doi.org/10.3389/fbioe.2020.00374>.
- [17] A. Fernandez-Colino, D.A. Quinteros, D.A. Allemandi, A. Girotti, S.D. Palma, F. J. Arias, Self-assembling elastin-like hydrogels for timolol delivery: development of an ophthalmic formulation against glaucoma, Mol. Pharm. 14 (2017) 4498–4508, <https://doi.org/10.1021/acs.molpharmaceut.7b00615>.
- [18] M.J. Pina, A. Girotti, S. Serrano, R. Muñoz, J.C. Rodriguez-Cabello, F.J. Arias, A double safety lock tumor-specific device for suicide gene therapy in breast cancer, Cancer Lett. 470 (2020) 43–53, <https://doi.org/10.1016/j.canlet.2019.11.031>.
- [19] L.C. Cantley, The phosphoinositide 3-kinase pathway, Science. 296 (2002) 1655–1657, <https://doi.org/10.1126/science.296.5573.1655>.
- [20] J. Luo, B.D. Manning, L.C. Cantley, Targeting the PI3K-Akt pathway in human cancer: rationale and promise, Cancer Cell 4 (2003) 257–262, [https://doi.org/10.1016/s1535-6108\(03\)00248-4](https://doi.org/10.1016/s1535-6108(03)00248-4).
- [21] J. Gonzalez-Valdivieso, A. Garcia-Sampedro, A.R. Hall, A. Girotti, F.J. Arias, S. P. Pereira, P. Acedo, Smart nanoparticles as advanced anti-Akt kinase delivery systems for pancreatic cancer therapy, ACS Appl. Mater. Interfaces 13 (2021) 55790–55805, <https://doi.org/10.1021/acsami.1c14592>.
- [22] J. Gonzalez-Valdivieso, A. Girotti, R. Muñoz, J.C. Rodriguez-Cabello, F.J. Arias, Self-assembling ELR-based nanoparticles as smart drug-delivery systems modulating cellular growth via Akt, Biomacromolecules. 20 (2019) 1996–2007, <https://doi.org/10.1021/acs.biomac.9b00206>.
- [23] M. Hirumura, F. Okada, T. Obata, D. Auguin, T. Shibata, C. Roumestand, M. Noguchi, Inhibition of Akt kinase activity by a peptide spanning the betaA strand of the proto-oncogene TCL1, J. Biol. Chem. 279 (2004) 53407–53418, <https://doi.org/10.1074/jbc.M403775200>.
- [24] R. Fan, Y. Wang, B. Han, Y. Luo, L. Zhou, X. Peng, M. Wu, Y. Zheng, G. Guo, Docetaxel load biodegradable porous microspheres for the treatment of colorectal peritoneal carcinomatosis, Int. J. Biol. Macromol. 69 (2014) 100–107, <https://doi.org/10.1016/j.ijbiomac.2014.05.026>.
- [25] J.M. Lee, H. Park, K.T. Oh, E.S. Lee, pH-Responsive hyaluronated liposomes for docetaxel delivery, Int. J. Pharm. 547 (2018) 377–384, <https://doi.org/10.1016/j.ijpharm.2018.06.028>.
- [26] A. Kadari, D. Pooja, R.H. Gora, S. Gudem, V.R.M. Kolapalli, H. Kulhari, R. Sistla, Design of multifunctional peptide collaborated and docetaxel loaded lipid nanoparticles for anti glioma therapy, Eur. J. Pharm. Biopharm. 132 (2018) 168–179, <https://doi.org/10.1016/j.ejpb.2018.09.012>.
- [27] V. Kushwah, S.S. Katiyar, A.K. Agrawal, R.C. Gupta, S. Jain, Co-delivery of docetaxel and gemcitabine using PEGylated self-assembled stealth nanoparticles for improved breast cancer therapy, Nanomedicine. 14 (2018) 1629–1641, <https://doi.org/10.1016/j.nano.2018.04.009>.
- [28] P.E. Saw, M. Yu, M. Choi, E. Lee, S. Jon, O.C. Farokhzad, Hyper-cell-permeable micelles as a drug delivery carrier for effective cancer therapy, Biomaterials. 123 (2017) 118–126, <https://doi.org/10.1016/j.biomaterials.2017.01.040>.
- [29] A. Girotti, A. Fernandez-Colino, I.M. Lopez, J.C. Rodriguez-Cabello, F.J. Arias, Elastin-like recombinamers: biosynthetic strategies and biotechnological applications, Biotechnol. J. 6 (2011) 1174–1186, <https://doi.org/10.1002/biot.201100116>.
- [30] R.E. Sallach, W. Cui, F. Balderrama, A.W. Martinez, J. Wen, C.A. Haller, J. V. Taylor, E.R. Wright, R.C. Long, E.L. Chaikof, Long-term biostability of self-

- assembling protein polymers in the absence of covalent crosslinking, *Biomaterials*. 31 (2010) 779–791, <https://doi.org/10.1016/j.biomaterials.2009.09.082>.
- [31] R. Vallejo, J. Gonzalez-Valdivieso, M. Santos, S. Rodriguez-Rojo, F.J. Arias, Production of elastin-like recombinamer-based nanoparticles for docetaxel encapsulation and use as smart drug-delivery systems using a supercritical anti-solvent process, *J. Ind. Eng. Chem.* 93 (2020) 361–374, <https://doi.org/10.1016/j.jiec.2020.10.013>.
- [32] C. Neufert, C. Becker, M.F. Neurath, An inducible mouse model of colon carcinogenesis for the analysis of sporadic and inflammation-driven tumor progression, *Nat. Protoc.* 2 (2007) 1998–2004, <https://doi.org/10.1038/nprot.2007.279>.
- [33] G. Battogtokh, O. Gotov, J.H. Kang, J. Cho, T.H. Jeong, G. Chimed, Y.T. Ko, Triphenylphosphine-docetaxel conjugate-incorporated albumin nanoparticles for cancer treatment, *Nanomedicine*. 13 (2018) 325–338, <https://doi.org/10.2217/nmm-2017-0274>.
- [34] C. Chen, S. Zhao, A. Karnad, J.W. Freeman, The biology and role of CD44 in cancer progression: therapeutic implications, *J. Hematol. Oncol.* 11 (2018) 64, <https://doi.org/10.1186/s13045-018-0605-5>.
- [35] V.J. Wielenga, R. van der Neut, G.J. Offerhaus, S.T. Pals, CD44 glycoproteins in colorectal cancer: expression, function, and prognostic value, *Adv. Cancer Res.* 77 (2000) 169–187, [https://doi.org/10.1016/s0065-230x\(08\)60787-3](https://doi.org/10.1016/s0065-230x(08)60787-3).
- [36] V. Orian-Rousseau, J. Sleeman, CD44 is a multidomain signaling platform that integrates extracellular matrix cues with growth factor and cytokine signals, *Adv. Cancer Res.* 123 (2014) 231–254, <https://doi.org/10.1016/b978-0-12-800092-2.00009-5>.
- [37] M. Zoller, CD44: can a cancer-initiating cell profit from an abundantly expressed molecule? *Nat. Rev. Cancer* 11 (2011) 254–267, <https://doi.org/10.1038/nrc3023>.
- [38] A.D. Keefe, S. Pai, A. Ellington, Aptamers as therapeutics, *Nat. Rev. Drug Discov.* 9 (2010) 537–550, <https://doi.org/10.1038/nrd3141>.
- [39] R. Stoltenberg, C. Reinemann, B. Strehlitz, SELEX—a (r)evolutionary method to generate high-affinity nucleic acid ligands, *Biomol. Eng.* 24 (2007) 381–403, <https://doi.org/10.1016/j.bioeng.2007.06.001>.
- [40] H.Y. Jeong, S.H. Baek, S.J. Chang, S.A. Cheon, T.J. Park, Robust fluorescence sensing platform for detection of CD44 cells based on graphene oxide/gold nanoparticles, *Colloids Surf. B: Biointerfaces* 135 (2015) 309–315, <https://doi.org/10.1016/j.colsurfb.2015.07.083>.
- [41] S. Moreno-Estar, S. Serrano, M. Arevalo-Martinez, P. Ciudad, J.R. Lopez-Lopez, M. Santos, M.T. Perez-Garcia, F.J. Arias, Elastin-like recombinamer-based devices releasing Kv1.3 blockers for the prevention of intimal hyperplasia: an in vitro and in vivo study, *Acta Biomater.* 115 (2020) 264–274, <https://doi.org/10.1016/j.actbio.2020.07.053>.
- [42] R. Li, Z. Xu, Q. Jiang, Y. Zheng, Z. Chen, X. Chen, Characterization and biological evaluation of a novel silver nanoparticle-loaded collagen-chitosan dressing, *Regen. Biomater.* 7 (2020) 371–380, <https://doi.org/10.1093/rb/rbaa008>.
- [43] Y. Matsumura, H. Maeda, A new concept for macromolecular therapeutics in cancer chemotherapy: mechanism of tumorotropic accumulation of proteins and the antitumor agent smancs, *Cancer Res.* 46 (1986) 6387–6392.
- [44] R.R. Arvizo, O.R. Miranda, M.A. Thompson, C.M. Pabelick, R. Bhattacharya, J. D. Robertson, V.M. Rotello, Y.S. Prakash, P. Mukherjee, Effect of nanoparticle surface charge at the plasma membrane and beyond, *Nano Lett.* 10 (2010) 2543–2548, <https://doi.org/10.1021/nl101140t>.
- [45] G. Fanali, A. di Masi, V. Trezza, M. Marino, M. Fasano, P. Ascenzi, Human serum albumin: from bench to bedside, *Mol. Asp. Med.* 33 (2012) 209–290, <https://doi.org/10.1016/j.mam.2011.12.002>.
- [46] K. Cho, X. Wang, S. Nie, Z.G. Chen, D.M. Shin, Therapeutic nanoparticles for drug delivery in cancer, *Clin. Cancer Res.* 14 (2008) 1310–1316, <https://doi.org/10.1158/1078-0432.ccr-07-1441>.
- [47] Q. Tan, X. Liu, X. Fu, Q. Li, J. Dou, G. Zhai, Current development in nanoformulations of docetaxel, *Expert Opin. Drug Deliv.* 9 (2012) 975–990, <https://doi.org/10.1517/17425247.2012.696606>.
- [48] H. Hernandez-Vargas, J. Palacios, G. Moreno-Bueno, Molecular profiling of docetaxel cytotoxicity in breast cancer cells: uncoupling of aberrant mitosis and apoptosis, *Oncogene*. 26 (2007) 2902–2913, <https://doi.org/10.1038/sj.onc.1210102>.
- [49] F. Impens, P. Van Damme, H. Demol, J. Van Damme, J. Vandekerckhove, K. Gevaert, Mechanistic insight into taxol-induced cell death, *Oncogene*. 27 (2008) 4580–4591, <https://doi.org/10.1038/nc.2008.96>.
- [50] M. Mediavilla-Varela, F.J. Pacheco, F. Almaguel, J. Perez, E. Sahakian, T. R. Daniels, L.S. Leoh, A. Padilla, N.R. Wall, M.B. Lilly, M. De Leon, C.A. Casiano, Docetaxel-induced prostate cancer cell death involves concomitant activation of caspase and lysosomal pathways and is attenuated by LEDGF/p75, *Mol. Cancer* 8 (2009) 68, <https://doi.org/10.1186/1476-4598-8-68>.
- [51] S.R. MacEwan, A. Chilkoti, From composition to cure: a systems engineering approach to anticancer drug carriers, *Angew. Chem. Int. Ed. Eng.* 56 (2017) 6712–6733, <https://doi.org/10.1002/anie.201610819>.
- [52] P. Shi, J.A. Gustafson, J.A. MacKay, Genetically engineered nanocarriers for drug delivery, *Int. J. Nanomedicine* 9 (2014) 1617–1626, <https://doi.org/10.2147/ijn.s53886>.
- [53] J. Hu, G. Wang, X. Liu, W. Gao, Enhancing pharmacokinetics, tumor accumulation, and antitumor efficacy by elastin-like polypeptide fusion of interferon alpha, *Adv. Mater.* 27 (2015) 7320–7324, <https://doi.org/10.1002/adma.201503440>.
- [54] P. Shi, S. Aluri, Y.A. Lin, M. Shah, M. Edman, J. Dhandhukia, H. Cui, J.A. MacKay, Elastin-based protein polymer nanoparticles carrying drug at both corona and core suppress tumor growth in vivo, *J. Control. Release* 171 (2013) 330–338, <https://doi.org/10.1016/j.jconrel.2013.05.013>.
- [55] J.A. MacKay, M. Chen, J.R. McDaniel, W. Liu, A.J. Sinnick, A. Chilkoti, Self-assembling chimeric polypeptide-doxorubicin conjugate nanoparticles that abolish tumours after a single injection, *Nat. Mater.* 8 (2009) 993–999, <https://doi.org/10.1038/nmat2569>.
- [56] M. De Robertis, E. Massi, M.L. Poeta, S. Carotti, S. Morini, L. Cecchetelli, E. Signori, V.M. Fazio, The AOM/DSS murine model for the study of colon carcinogenesis: from pathways to diagnosis and therapy studies, *J. Carcinog.* 10 (2011) 9, <https://doi.org/10.4103/1477-3163.78279>.
- [57] D. Mustafi, X. Fan, U. Dougherty, M. Bissonnette, G.S. Karczmar, A. Oto, J. Hart, E. Markiewicz, M. Zamora, High-resolution magnetic resonance colonography and dynamic contrast-enhanced magnetic resonance imaging in a murine model of colitis, *Magn. Reson. Med.* 63 (2010) 922–929, <https://doi.org/10.1002/mrm.22229>.
- [58] M.M. Badran, A.H. Alomrani, G.I. Harisa, A.E. Ashour, A. Kumar, A.E. Yassin, Novel docetaxel chitosan-coated PLGA/PCL nanoparticles with magnified cytotoxicity and bioavailability, *Biomed. Pharmacother.* 106 (2018) 1461–1468, <https://doi.org/10.1016/j.biopha.2018.07.102>.
- [59] P. Zahedi, R. De Souza, M. Piquette-Miller, C. Allen, Chitosan-phospholipid blend for sustained and localized delivery of docetaxel to the peritoneal cavity, *Int. J. Pharm.* 377 (2009) 76–84, <https://doi.org/10.1016/j.ijpharm.2009.05.003>.
- [60] C. Becker, M.C. Fantini, C. Schramm, H.A. Lehr, S. Wirtz, A. Nikolaev, J. Burg, S. Strand, R. Kiesslich, S. Huber, H. Ito, N. Nishimoto, K. Yoshizaki, T. Kishimoto, P.R. Galle, M. Blessing, S. Rose-John, M.F. Neurath, TGF-beta suppresses tumor progression in colon cancer by inhibition of IL-6 trans-signaling, *Immunity*. 21 (2004) 491–501, <https://doi.org/10.1016/j.immuni.2004.07.020>.
- [61] G.P. Boivin, K. Washington, K. Yang, J.M. Ward, T.P. Pretlow, R. Russell, D. G. Besselsen, V.L. Godfrey, T. Doetschman, W.F. Dove, H.C. Pitot, R.B. Halberg, S. H. Itzkowitz, J. Groden, R.J. Coffey, Pathology of mouse models of intestinal cancer: consensus report and recommendations, *Gastroenterology*. 124 (2003) 762–777, <https://doi.org/10.1053/gast.2003.50094>.
- [62] J. Gonzalez-Valdivieso, A. Girotti, J. Schneider, F.J. Arias, Advanced nanomedicine and cancer: challenges and opportunities in clinical translation, *Int. J. Pharm.* 599 (2021), 120438, <https://doi.org/10.1016/j.ijpharm.2021.120438>.